

Relationship between meteoric ^{10}Be and NO_3^- concentrations in soils along Shackleton Glacier, Antarctica

Melisa A. Diaz^{1,2†}, Lee B. Corbett³, Paul R. Bierman³, Byron J. Adams⁴, Diana H. Wall⁵, Ian D. Hogg^{6,7}, Noah Fierer⁸, W. Berry Lyons^{1,2}

¹School of Earth Sciences, The Ohio State University, Columbus, OH, 43210, USA

²Byrd Polar and Climate Research Center, The Ohio State University, Columbus, OH, 43210, USA

³Department of Geology, University of Vermont, Burlington, VT, 05405, USA

⁴Department of Biology, Evolutionary Ecology Laboratories, and Monte L. Bean Museum, Brigham Young University, Provo, UT, 84602, USA

⁵Department of Biology and School of Global Environmental Sustainability, Colorado State University, Fort Collins, CO, 80523, USA

⁶Canadian High Arctic Research Station, Polar Knowledge Canada, Cambridge Bay, NU, X0B0C0, Canada

⁷School of Science, University of Waikato, Hamilton, 3216, New Zealand

⁸Department of Ecology and Evolutionary Biology and Cooperative Institute for Research in Environmental Science, University of Colorado Boulder, Boulder, CO, 80309, USA

[†]Now at Departments of Geology and Geophysics, and Applied Ocean Physics and Engineering, Woods Hole Oceanographic Institution, Woods Hole, MA, 02543, USA

Correspondence to: Melisa A. Diaz (mdiaz@whoi.edu)

Abstract. Outlet glaciers that flow through the Transantarctic Mountains (TAM) experienced changes in ice thickness greater than other coastal regions of Antarctica during glacial maxima. As a result, ice-free areas that are currently exposed may have been covered by ice at various points during the Cenozoic, complicating our understanding of ecological succession in TAM soils. Our knowledge of glacial extent on small spatial scales is limited for the TAM, and studies of soil exposure duration and disturbance, in particular, are rare. We collected surface soil samples, and in some places, depth profiles every 5 cm to refusal (up to 30 cm) from eleven ice-free areas along Shackleton Glacier, a major outlet glacier of the East Antarctic Ice Sheet. We explored the relationship between meteoric ^{10}Be and NO_3^- in these soils as a tool for understanding landscape disturbance and wetting history, and as exposure proxies. Concentrations of meteoric ^{10}Be spanned more than an order of magnitude across the region (2.9×10^8 atoms g^{-1} to 73×10^8 atoms g^{-1}) and are among the highest measured in polar regions. The concentrations of NO_3^- were similarly variable and ranged from $\sim 1 \mu\text{g g}^{-1}$ to 15mg g^{-1} . In examining differences and similarities in the concentrations of ^{10}Be and NO_3^- with depth, we suggest that much of the southern portion of the Shackleton Glacier region has likely developed under a hyper-arid climate regime with minimal disturbance. Finally, we inferred exposure time using ^{10}Be concentrations. This analysis indicates that the soils we analyzed likely range from recent exposure (following the Last Glacial Maximum) to possibly >6 Ma. We suggest that further testing and interrogation of meteoric ^{10}Be and NO_3^- concentrations and relationships in soils can provide important information regarding landscape development, soil evolution processes, and inferred exposure durations of surfaces in the TAM.

39 **1. Introduction**

40 One of the most intriguing questions in biogeography concerns the relationship between the evolution of
41 terrestrial organisms and landscape disturbance (e.g., glacial overriding, soil wetting), particularly in Antarctica.
42 Current data indicate that organism lineages have survived in some Antarctic soils for possibly millions of years,
43 despite multiple glaciations throughout the Pleistocene (Convey et al., 2008; Fraser et al., 2012; Stevens and Hogg,
44 2003). It is still unclear how and where these organisms found suitable glacial refugia given the high salt
45 concentrations in high-elevation soils (Lyons et al., 2016). The most biodiverse soils in the Ross Sea sector are at
46 low elevations near the coast, where the Ross Ice Shelf or sea ice meet the Transantarctic Mountains (TAM) (Collins
47 et al., 2020). These soils are also those which are most susceptible to glacial overriding during glacial maxima,
48 though the timing of retreat and glacial extent is still unknown on local scales (Golledge et al., 2012; Mackintosh et
49 al., 2011).

50 Outlet glaciers are among the most responsive cryospheric components in Antarctica, and changes in their
51 extents over time are recorded in nearby sedimentary deposits (Golledge et al., 2013; Jones et al., 2015; Scherer et
52 al., 2016; Spector et al., 2017). However, only scattered information exists on TAM soil processes, ages and
53 chronosequences, and their implications for terrestrial and ecosystem history (Bockheim, 2002; Dickinson et al.,
54 2012; Graham et al., 2002, 1997; Lyons et al., 2016; Scarrow et al., 2014; Schiller et al., 2009). Shackleton Glacier,
55 an outlet glacier of the East Antarctic Ice Sheet (EAIS), flows between several exposed peaks of the Central
56 Transantarctic Mountains (CTAM) and ice-free areas are present at both low and high elevations. We report
57 concentrations of meteoric ^{10}Be and nitrate (NO_3^-) in soils from eleven ice-free areas and investigate their
58 distributions at depth to explore ^{10}Be and NO_3^- relationships. The sampling methodology was designed to capture a
59 range of soils which have low salt concentrations due to recent exposure from glacial retreat following the Last
60 Glacial Maximum (LGM) and soils that were likely exposed since at least the last glacial period. These data include
61 some of the only meteoric ^{10}Be and NO_3^- concentration data from the CTAM (Claridge and Campbell, 1968b, 1977;
62 Graham et al., 1997; Lyons et al., 2016), inform knowledge of landscape disturbance and wetting history, may
63 potentially be used to infer soil exposure duration, and are useful in understanding Antarctic terrestrial
64 biogeography.

65 **2. Background**

66 **2.1. Brief overview of Antarctic glacial and wetting history**

67 Antarctica is believed to have maintained a persistent ice sheet since at least the Eocene epoch, where
68 paleorecords indicate that the East and West Antarctic Ice Sheets (EAIS and WAIS, respectively) have waxed and
69 waned since at least the Miocene (Gasson et al., 2016; Gulick et al., 2017). Sediment core records collected from the
70 Ross Sea and ice cores from the Antarctic interior indicate that the EAIS and WAIS have undergone dozens of
71 glacial and interglacial cycles throughout the Cenozoic (Augustin et al., 2004; Talarico et al., 2012). The WAIS is a
72 marine-terminating ice sheet defined by a grounding line below sea level, which decreases the stability of the ice
73 sheet and results in more rapid advance and retreat compared to the EAIS (Pollard and DeConto, 2009). The EAIS is
74 grounded above sea level and is therefore generally more stable. The EAIS and WAIS were at their most recent
75 greatest extent about 14 ka during the LGM (Clark et al., 2009). During the LGM, the EAIS expanded along its
76 margins and some of the greatest increases in height occurred at outlet glaciers which flow through exposed peaks of
77 the TAM and drain into the Ross and Weddell seas (Anderson et al., 2002; Golledge et al., 2012; Mackintosh et al.,
78 2014). As a result, many of the currently exposed TAM soils were overrun by ice during the LGM and some may
79 have only recently been exposed.

80 Much of the Antarctic continent is a polar desert and geomorphological data from ice-free soils in the
81 McMurdo Dry Valleys indicate that some regions have likely been hyper-arid for as long as 15 Ma (Marchant et al.,
82 1996; Valletta et al., 2015). As such, atmospherically-derived constituents, including salts and metals, can
83 accumulate in exposed Antarctic soils at concentrations similar to those from the Atacama and Namib Deserts (Diaz
84 et al., 2020; Lyons et al., 2016; Reich and Bao, 2018). Using soil NO_3^- concentrations from the Meyer Desert in the

85 Beardmore Glacier region and NO_3^- fluxes calculated from a Dominion Range ice core, Lyons et al. (2016)
86 estimated that at least 750,000 years have passed since the Meyer Desert had wide-spread soil wetting. It is likely
87 that other high elevation and inland locations in the TAM also have high concentrations of salts and similarly old
88 “wetting ages”, though this has not been thoroughly investigated.

89 2.2. Meteoric ^{10}Be systematics in Antarctic soils

90 ^{10}Be is a cosmogenic radionuclide with a half-life of 1.39 Ma (Korschinek et al., 2010) that is produced
91 both in the atmosphere (meteoric) and *in-situ* in mineral grains. In the atmosphere, N and O gases are bombarded by
92 high energy cosmic radiation to produce meteoric ^{10}Be . Particle reactive ^{10}BeO or $^{10}\text{Be}(\text{OH})_2$ is produced and
93 removed from the atmosphere by wet and dry deposition (McHargue and Damon, 1991). At Earth’s surface,
94 meteoric ^{10}Be sorbs onto clay particles and is insoluble in most natural waters of pH greater than 4 (Brown et al.,
95 1992; You et al., 1989). The clay particles can be redistributed to lower depths in soils due to particle migration or
96 can be transported by winds. As such, the total number of ^{10}Be atoms in a soil profile, its inventory, is a function of
97 surface exposure duration, erosion, clay particle translocation, solubility, and sedimentation. If delivery rates can be
98 determined, meteoric ^{10}Be can be used as a tool to understand exposure ages, erosion rates, and soil residence times
99 (see Willenbring and Von Blanckenburg, 2009 and references within). There are scattered exposure age studies from
100 across the CTAM using a variety of *in-situ* produced cosmogenic nuclides (Ackert and Kurz, 2004; Balter-Kennedy
101 et al., 2020; Bromley et al., 2010; Kaplan et al., 2017; Spector et al., 2017), and previously reported exposure ages
102 of CTAM moraines and boulders from these studies ranged from <10 ka to >14 Ma.

103 The measurement of meteoric ^{10}Be in soil has enabled researchers to date surfaces (soils) and features in
104 Antarctica. Previous studies have measured meteoric ^{10}Be in the McMurdo Dry Valleys (MDV) and Victoria Land
105 soils and sediments to calculate exposure ages and to determine the onset of the current polar desert regime
106 (Dickinson et al., 2012; Graham et al., 2002; Schiller et al., 2009; Valletta et al., 2015). In general, these previous
107 studies found that high elevation, northern fringe regions along the Ross Embayment have been ice-free and
108 possibly hyper-arid since at least the Pliocene. Few meteoric ^{10}Be data have been previously published from the
109 CTAM (Graham et al., 1997), which represent ice sheet dynamics and climatic conditions closer to the Polar
110 Plateau.

111 2.3. Nitrate systematics in Antarctic soils

112 The nitrogen cycle in Antarctica differs greatly from the nitrogen cycle in temperate regions, primarily due
113 to scarce biomass and few vascular plants (Cary et al., 2010; Michalski et al., 2005). Nitrogen in CTAM soils
114 primarily exists as NO_3^- and is sourced from the atmosphere, with varying contributions from the troposphere and
115 stratosphere (Diaz et al., 2020; Lyons et al., 2016; Michalski et al., 2005). Similar to meteoric ^{10}Be , NO_3^- is
116 deposited on exposed soils, however, nitrate salts are highly water-soluble. Once deposited on the surface, nitrate
117 salts can be dissolved and transported down gradient or eluted to depth when wetted (i.e., during ice/snow melt
118 events). However, the hyper-arid climate of the CTAM can allow NO_3^- to accumulate at high concentrations in soils
119 (Claridge and Campbell, 1968a; Diaz et al., 2020; Lyons et al., 2016). Soil NO_3^- concentrations have the potential to
120 inform our knowledge of wetting history and possibly glacial history in the CTAM due to the relatively high
121 solubility of nitrate salts, though uncertainties regarding heterogeneous deposition and post-depositional alteration
122 (such as re-volatilization and photolysis) require further investigation (Diaz et al., 2020; Frey et al., 2009; Graham et
123 al., 2002).

124 3. Study sites and region

125 Shackleton Glacier (~84.5 to 86.4°S; ~130 km long and ~10 km wide) is a major outlet glacier of the EAIS
126 that drains north into the Ross Embayment with other CTAM outlet glaciers to form the Ross Ice Shelf (RIS) (Fig.
127 1). The ice flows between exposed surfaces of the Queen Maud Mountains, which range from elevations of ~150
128 m.a.s.l. near the RIS to >3,500 m.a.s.l. further inland. The basement geology of the Shackleton Glacier region is
129 comprised of igneous and metamorphic rocks that formed from intruded and metamorphosed sedimentary and
130 volcanic strata during the Ross Orogeny (450-520 Ma) (Elliot and Fanning, 2008). The southern portion of the

131 region consists of the Devonian-Triassic Beacon Supergroup and the Jurassic Ferrar Group, while the northern
132 portions consists of Pre-Devonian granitoids and the Early to Mid-Cambrian Taylor Group (Elliot and Fanning,
133 2008; Paulsen et al., 2004). These rocks serve as primary parent material for soil formation (Claridge and Campbell,
134 1968b). Deposits of the Sirius Group, the center of the stable vs. dynamic EAIS debate (Barrett, 2013; Sugden et al.,
135 1993; Webb et al., 1984; Wilson, 1995), have been previously identified in the southern portion of the Shackleton
136 Glacier region, particularly at Roberts Massif (Fig. 2) and Bennett Platform, with a small exposure at Schroeder Hill
137 (Hambrey et al., 2003).

138 The valleys and other ice-free areas within the region have been modified by the advance and retreat of
139 Shackleton Glacier, smaller tributary glaciers, and alpine glaciers. Similar to the Beardmore Glacier region, the
140 Shackleton Glacier region is a polar desert, which results in the high accumulation of salts in soils. The surface is
141 comprised primarily of till, weathered primary bedrock, and scree, which ranges in size from small boulders and
142 cobbles to sand and silt. Clay minerals have been previously identified in all samples from Roberts Massif and are
143 likely ubiquitous throughout the region (Claridge and Campbell, 1968b). The clays are a mixture of those derived
144 from sedimentary rocks and contemporaneous weathering (Claridge and Campbell, 1968b). Thin, boulder belt
145 moraines, characteristic of cold-based glaciers, were deposited over bedrock and tills at Roberts Massif, while large
146 moraines were deposited at Bennett Platform (Fig. 2; Balter-Kennedy et al., 2020; Claridge and Campbell, 1968).
147 Most soils appeared dry, though some small ponds and water tracks have been documented near Mt. Heekin and
148 Thanksgiving Valley (Elliot et al., 1996). Additional information on the sample locations and surface features is
149 provided in Tables 1 and 2.

150 **4. Methods**

151 **4.1. Sample collection**

152 During the 2017-2018 austral summer, we visited eleven ice-free areas along Shackleton Glacier: Roberts
153 Massif, Schroeder Hill, Bennett Platform, Mt. Augustana, Mt. Heekin, Thanksgiving Valley, Taylor Nunatak, Mt.
154 Franke, Mt. Wasko, Nilsen Peak, and Mt. Speed (Fig. 1). These areas represent soils from near the head of the
155 glacier to near the glacier terminus at the coast of the RIS. Two surface samples (Table 1) were collected at each
156 location (except for Nilsen Peak and Mt. Wasko, represented by only one sample each) with a plastic scoop and
157 stored in Whirl-Pak™ bags. One sample was collected furthest from Shackleton Glacier or other tributary glaciers
158 (within ~2,000 m) to represent soils that were likely exposed during the LGM and previous recent glacial periods. A
159 second sample was collected closer to the glacier (between ~1,500 and 200 m from the first sample) to represent
160 soils likely to have been covered during the LGM and exposed by more recent ice margin retreat.

161 Soil pits were dug by hand at the sampling locations furthest from the glacier for Roberts Massif, Schroeder
162 Hill, Mt. Augustana, Bennett Platform, Mt. Heekin, Thanksgiving Valley, and Mt. Franke (7 sites). Continuous
163 samples were collected every 5 cm until refusal (up to 30 cm) and stored frozen in Whirl-Pak™ bags. All surface
164 (21) and depth profile (25) samples were shipped frozen to The Ohio State University and kept frozen until
165 analyzed. We selected Roberts Massif, Bennett Platform, and Thanksgiving Valley as locations for the most in-
166 depth analysis for the depth profiles. These locations were chosen to maximize variability in landscape
167 development: Roberts Massif represented an older, likely minimally disturbed landscape; Bennett Platform
168 represented a landscape with evidence of recent glacial advance and retreat, and substantial topographic highs and
169 lows; Thanksgiving Valley represented a landscape with possible hydrologic activity, as evidenced by nearby ponds
170 (Table 2).

171 **4.2. Analytical methods**

172 **4.2.1. Meteoric ¹⁰Be analysis**

173 A total of 30 sub-samples of surface soils from all locations, and the depth profiles from Roberts Massif,
174 Bennett Platform, and Thanksgiving Valley, were sieved to determine the grain size at each location. For each
175 sample, the percentages of gravel (>2 mm), sand (63 μm-2 mm), and silt (<63 μm) are reported in Table S1. Since
176 there is a strong grain size dependence of meteoric ¹⁰Be (little ¹⁰Be is carried on coarse (>2 mm) grains (Pavich et

177 al., 1986)), the gravel portion of the sample was not included in the meteoric ^{10}Be analysis. The remaining soil (<2
178 mm) was ground to fine powder using a shatterbox.

179 Meteoric ^{10}Be (Table 1; S2) was extracted and purified at the NSF/University of Vermont (UVM)
180 Community Cosmogenic Facility following procedures adapted from Stone (1998). First, 0.5 g of powdered soil was
181 weighed into platinum crucibles and 0.4 g of SPEX ^9Be carrier (with a concentration of $1,000 \mu\text{g mL}^{-1}$) was added to
182 each sample. The samples were fluxed with a mixture of potassium hydrogen fluoride and sodium sulfate. Perchloric
183 acid was then added to remove potassium by precipitation and later evaporated. Samples were dissolved in nitric
184 acid and precipitated as beryllium hydroxide ($\text{Be}(\text{OH})_2$) gel, then packed into stainless steel cathodes for accelerator
185 mass spectrometer isotopic analysis at the Purdue Rare Isotope Measurement (PRIME) Laboratory. Isotopic ratios
186 were normalized to primary standard 07KNSTD with an assumed ratio of 2.85×10^{-12} (Nishiizumi et al., 2007). We
187 corrected sample ratios with a $^{10}\text{Be}/^9\text{Be}$ blank ratio of $8.2 \pm 1.9 \times 10^{-15}$, which is the average standard deviation of
188 two blanks processed alongside the samples. We subtracted the blank ratio from the sample ratios and propagated
189 uncertainties in quadrature. Blank correction is not significant.

190 4.2.2. NO_3^- analysis

191 Separate, un-sieved sub-samples of soil from all locations and depth profiles were leached at a 1:5 soil to
192 DI water ratio for 24 hours, then filtered through a $0.4 \mu\text{m}$ Nuclepore membrane filter. The leachate was analyzed on
193 a Skalar San++ Automated Wet Chemistry Analyzer with an SA 1050 Random Access Auto-sampler (Lyons et al.,
194 2016; Welch et al., 2010). Concentrations are reported as NO_3^- (Table 1) with accuracy, as determined using a
195 USGS 2015 “round-robin” standard, and precision better than 5% (Lyons et al., 2016).

196 4.3. Meteoric ^{10}Be inventory

197 We developed a mass balance using the fluxes of meteoric ^{10}Be to and from Shackleton Glacier region soils
198 to understand the accumulation of ^{10}Be in glaciated environments (Pavich et al., 1984, 1986). The model assumes
199 that soils that were overlain by glacial ice in the past and are now exposed, accumulated less ^{10}Be than soils that
200 were exposed throughout the glacial periods (Fig. 3). The concentration of meteoric ^{10}Be at the surface (N , atoms g^{-1})
201 per unit of time (dt) is expressed as a function, where the addition of ^{10}Be is represented as the atmospheric flux to
202 the surface (Q , atoms $\text{cm}^{-2} \text{yr}^{-1}$), and removal is due to both radioactive decay, which is represented by a
203 disintegration constant (λ , yr^{-1}), and erosion (E , cm yr^{-1}) (Eq. 1). Particle mobility into the soil column is represented
204 by a diffusion constant (D , $\text{cm}^2 \text{yr}^{-1}$). The differential in depth is represented by dz .

$$205 \frac{dN}{dt} = Q - \lambda N - E \frac{dN}{dz} - D \frac{d^2N}{dz^2} \quad (1)$$

206 We accounted for uncertainties regarding ^{10}Be migration in the soil column by calculating the inventory (I ,
207 atoms cm^{-2}) of the soil (Eq. 2) (Pavich et al., 1986). We used a density (ρ) of 2 g cm^{-3} and assumed that Q had not
208 changed systematically over the accumulation interval. The inventory is the total sum of meteoric ^{10}Be atoms in the
209 soil profile and the change in inventory due to deposition, decay, and surface erosion is related surface exposure
210 duration (Eq. 3).

$$211 I = \sum N \cdot \rho \cdot dz \quad (2)$$

$$212 \frac{dI}{dt} = Q - \lambda I - EN \quad (3)$$

213 Meteoric ^{10}Be concentrations typically decrease with depth until they reach a “background” level (Graly et
214 al., 2010). The background is identified as the point where the concentration of meteoric ^{10}Be is constant with depth
215 ($\frac{dN}{dz} = 0$). Typically, the background values can be used to calculate an initial inventory (I_i , atoms cm^{-2}) using Eq. 4,
216 where N_z is the ^{10}Be concentration (atoms g^{-1}) at the bottom of the profile (z , cm). In this case, we assume that the
217 initial concentration of meteoric ^{10}Be is isotropic. However, an accurate initial inventory can only be determined for

218 soil profiles that are deep enough to capture background concentrations. This may not be the case in areas of
219 permafrost where ^{10}Be is restricted to the active layer (Bierman et al., 2014).

$$220 \quad I_i = N_z \cdot \rho \cdot z \quad (4)$$

221 Additionally, the initial inventory can be influenced by repeated glacier advance and retreat during glacial-
222 interglacial cycles. For this case, the soil has “inherited” ^{10}Be during each subsequent exposure to the atmosphere,
223 some of which may have been removed with eroded soil (Fig. 3c-d). For constructional landforms, such as moraines,
224 the inheritance is equal to the background/initial inventory. Without information on drift sequences, it is difficult to
225 correct the measured inventory for inheritance by distinguishing meteoric ^{10}Be that was deposited after the most
226 recent ice retreat from ^{10}Be that was deposited during previous interglacial periods.

227 5. Results

228 5.1. Depth profile composition and concentrations of meteoric ^{10}Be

229 Sediment grain size is similar among the three soil profiles collected from Roberts Massif, Bennett
230 Platform, and Thanksgiving Valley; the soils are primarily comprised of sand-sized particles, with less silt-sized and
231 smaller material (Fig. 4). The proportions of silt and gravel are similar at Roberts Massif, although the majority of
232 the profile is sand-sized. Thanksgiving Valley has the coarsest material, while Bennett Platform has a more even
233 grain size distribution. The deepest profile is from Thanksgiving Valley, while the Roberts Massif and Bennett
234 Platform profiles are half the depth. All three profiles are ice-cemented at the bottom and are shallow compared
235 those collected from the McMurdo Dry Valleys (Dickinson et al., 2012; Schiller et al., 2009; Valletta et al., 2015),
236 though they are comparable to profiles collected at Roberts Massif by Graham et al. (1997).

237 Concentrations of meteoric ^{10}Be for both surface and depth profiles samples span more than an order of
238 magnitude in the Shackleton Glacier region and range from 2.9×10^8 atoms g^{-1} at Mount Speed to 73×10^8 atoms g^{-1}
239 at Roberts Massif (Fig. 5; Table 1). At individual sites where samples were collected at two locations,
240 concentrations are typically highest for the samples furthest from the glacier, with notable exceptions at Roberts
241 Massif and Thanksgiving Valley (Fig. 5). This trend is expected since our sampling plan was designed to capture
242 both recently exposed soils (near the glacier(s)) and soils which have been exposed throughout the LGM and
243 possibly other glacial periods. The measured inventories (Eq. 2) vary from 0.57×10^{11} atoms at Bennett Platform to
244 1.5×10^{11} atoms at Roberts Massif (Table 3).

245 The meteoric ^{10}Be depth profiles differ between Roberts Massif, Bennett Platform, and Thanksgiving
246 Valley. The profile from Roberts Massif has the highest overall concentrations (Fig. 6). Within the profile, the 5-10
247 cm sampling interval has the highest concentration, followed by the bottom of the profile, then the surface. The
248 profile behavior for Thanksgiving Valley is similar, though the differences in concentrations within both profiles are
249 relatively small. Bennett Platform is the only location where the surface concentration is the highest compared to the
250 remainder of the profile and the concentration decreases with depth (Fig. 6). Although we sampled the entirety of
251 the active layer where modern particle mobility throughout the soil column occurs, no depth profiles appear to
252 decrease to background levels needed to calculate an initial meteoric ^{10}Be inventory (Eq. 4). As a result, we are not
253 able to correct the measured inventory for background ^{10}Be , nor are we able estimate the inherited ^{10}Be
254 concentration in the soil.

255 5.2. Variability of NO_3^-

256 Measured concentrations of NO_3^- span four orders of magnitude across the seven depth profiles we sampled
257 (Fig. 6; Table 1). The lowest concentration is from Mt. Franke, $\sim 1 \mu\text{g g}^{-1}$; the highest concentration is from Roberts
258 Massif, 15 mg g^{-1} . In addition, similar to the meteoric ^{10}Be profiles, the NO_3^- concentrations are highest for the
259 samples that were collected furthest from the coast and at the highest elevations (Table 1). In general, the profiles
260 from Roberts Massif and Thanksgiving Valley are similar (Fig. 6b); ^{10}Be and NO_3^- concentrations are highest just
261 below the surface in the 5-10 cm interval and are fairly consistent throughout the profile. The NO_3^- depth profile

262 mirrors the ^{10}Be profile at Bennett Platform – while ^{10}Be concentration decreases with depth, the NO_3^- concentration
263 increases with depth.

264 Since we measured NO_3^- concentrations for all seven depth profiles we collected, we compare the profile
265 concentrations and shapes from the four profiles without ^{10}Be depth measurements (Mt. Augustana, Schroeder Hill,
266 Mt. Franke, and Mt. Heekin) to the Roberts Massif, Bennett Platform, and Thanksgiving Valley profiles with both
267 measurements (Fig. 6). Most of the NO_3^- profiles do not significantly change with depth and are similar to the
268 profile from Thanksgiving Valley, though Schroeder Hill is most similar to Roberts Massif (Fig. 6). This is
269 unsurprising given the similar latitudes, surface features, and environmental conditions between the different
270 locations (e.g., high latitude hyper-arid vs. lower latitude with possible evidence of wetter conditions) (Fig. 1; Table
271 2). No other location had large terminal moraines, as observed at Bennett Platform.

272 **6. Discussion**

273 The Shackleton Glacier region soil profiles and surface samples are among the highest meteoric ^{10}Be
274 concentrations ($\sim 10^9$ atoms g^{-1}) yet measured in Earth's polar regions (Fig. 6a). Though our profiles are shallower
275 than profiles from the MDV and Victoria Land in Antarctica (Dickinson et al., 2012; Schiller et al., 2009; Valletta et
276 al., 2015) and Sweden and Alaska in the Arctic (Bierman et al., 2014; Ebert et al., 2012), the soils from these
277 previous studies reached background concentrations of ^{10}Be within the top 40 cm, which is close to our maximum
278 depth of 30 cm at Thanksgiving Valley. For comparison, the deepest profile collected by Graham et al. (1997) at
279 Roberts Massif was 36 cm. The Bennett Platform soil profile is most similar to the soil profiles from other regions in
280 Antarctica, as they have decreasing ^{10}Be concentrations with depth, while Thanksgiving Valley and Roberts Massif
281 are relatively homogenous and more similar to profiles from the Arctic.

282 The inventories from this study are also among the highest calculated for Antarctic soils. The inventories
283 from Bennett Platform and Thanksgiving Valley are most similar ($\sim 10^{10}$) to inventories of saprolites and tills from
284 Sweden (Ebert et al., 2012) and the MDV (Schiller et al., 2009), though higher than those measured from other high
285 elevation, inland locations in Victoria Land (Dickinson et al., 2012; Valletta et al., 2015). Our inventory from
286 Roberts Massif is the same as the inventory reported for a nearby location by Graham et al. (1997), and all of our
287 inventories are within the range of values from the Arctic (Bierman et al., 2014), despite shallower profiles.

288 **6.1. Relationships between meteoric ^{10}Be and NO_3^- and governing processes**

289 Previous studies have proposed that atmosphere-derived salt concentrations at the surface may correlate
290 with exposure ages and wetting ages in Antarctica (Everett, 1971; Graham et al., 2002, 1997; Graly et al., 2018;
291 Lyons et al., 2016; Schiller et al., 2009). Graly et al. (2018) showed that, in particular, water-soluble NO_3^- and boron
292 exhibited the strongest relationships with exposure age ($R^2 = 0.9$ and 0.99 , respectively). Lyons et al. (2016) used
293 NO_3^- concentrations to estimate the amount of time since the soils were last wetted, and Graham et al. (2002)
294 attempted to calculate exposure ages using the inventory of NO_3^- in the soil. Graly et al. (2018) argue that boron is
295 the preferable exposure proxy due to concerns related to NO_3^- mobility under sub-arid conditions (e.g. Frey et al.,
296 2009; Michalski et al., 2005), and given that uncertainties in local accumulation rates and ion transport can result in
297 inaccurate ages when using NO_3^- alone (Graham et al., 2002; Schiller et al., 2009). Based on the results presented
298 here for hyper-arid CTAM ice-free regions and the concerns with boron mobility depending on whether the B
299 species present in the soils is BO_3^{3-} (borate) or H_3BO_3 (boric acid), we suggest that NO_3^- is suitable for interpreting
300 wetting and disturbance histories.

301 Both meteoric ^{10}Be and NO_3^- are sourced from atmospheric deposition in the Shackleton Glacier region,
302 and there appears to be a relationship between the two constituents in the soil profiles (Fig. 6b). A similar
303 relationship between soluble salts and meteoric ^{10}Be was previously documented at Roberts Massif (Graham et al.,
304 1997). NO_3^- is highly mobile in wetter systems, while ^{10}Be is less mobile under circumneutral pH. Given sustained
305 hyper-arid conditions, minimal landscape disturbance, and negligible biologic activity, one can expect meteoric ^{10}Be
306 and NO_3^- to be correlated throughout a depth profile given the similar accumulation mechanism (Everett, 1971;

307 Graham et al., 1997). Further, their inventories (Eq. 2) should increase monotonically with exposure duration.
308 Deviations from this expected relationship could be due to 1) soil wetting, either in the present or past, 2) deposition
309 of sediment with different ^{10}Be to NO_3^- ratios compared to the depositional environment, 3) changes in the flux of
310 either ^{10}Be or NO_3^- with time, and 4) additional loss of NO_3^- due to denitrification or volatilization. The latter two
311 mechanisms are likely minor processes, however, NO_3^- deposition fluxes are known to be spatially variable (Jackson
312 et al., 2016; Lyons et al., 1990). As described above, Roberts Massif, Bennett Platform, and Thanksgiving Valley
313 were selected for further investigation as locations which may represent different depositional environments:
314 hypothesized hyper-aridity, recent glacial activity with large moraines, and active hydrology, respectively. By
315 comparing differences in the expected and observed relationship between ^{10}Be and NO_3^- , we can infer the processes
316 that have influenced their relationship.

317 **6.1.1. Implications for landscape disturbance and paleoclimate**

318 Our work demonstrates that NO_3^- and ^{10}Be are correlated in much of the Shackleton Glacier region, and the
319 soil profiles can inform our understanding of surficial processes and soil wetting for the region. Exposure age and
320 cosmogenic nuclide data from across Antarctica show that a polar desert regime began in the mid-Miocene and has
321 persisted into modern time (Lewis et al., 2008; Marchant et al., 1996; Spector and Balco, 2020; Valletta et al., 2015).
322 Additionally, Barrett (2013) provides a detailed review of studies focused on Antarctic glacial history, particularly
323 centered around the “stabilist vs. dynamicist” debate concerning the overall stability of the EAIS. Interpreting 40+
324 years of data from published literature, they conclude that the EAIS is stable in the interior with retreat occurring
325 along the margins, including at outlet glaciers (Golledge et al., 2012). Given these findings, we would expect NO_3^-
326 and meteoric ^{10}Be concentrations to be correlated in hyper-arid Antarctic soils, such as those from the Shackleton
327 Glacier region, as both constituents are derived from atmospheric deposition with minimal alteration at the surface.
328 The major differences between the two concern transport mechanisms; meteoric ^{10}Be transport is limited by clay
329 particle mobility and NO_3^- is mobile upon soil wetting.

330 If we assume an “ideal” situation where an undisturbed hyper-arid soil has accumulated meteoric ^{10}Be (Fig.
331 3a-b), ^{10}Be concentrations would be highest at the surface and eventually decrease to background levels at depth.
332 None of the profiles we sampled and measured for meteoric ^{10}Be and NO_3^- reached background concentrations. All
333 profiles had an active layer much shallower than those from the MDV (Graham et al., 2002; Schiller et al., 2009;
334 Valletta et al., 2015). This indicates that the active layer may have deepened and shallowed throughout time, and
335 modern ^{10}Be mobility is limited to the top ~20 cm for most of the Shackleton Glacier region. Though clay particle
336 translocation by percolating water can explain the correlated behavior of ^{10}Be and NO_3^- at Roberts Massif and
337 Thanksgiving Valley, it is unlikely that the region had sufficient precipitation for significant percolation over the last
338 14 Ma, given the high NO_3^- concentrations (Menziés et al., 2006). The concentrations of fine particles in the soil
339 profiles also do not change significantly with depth, as would be expected if large precipitation or melt events were
340 frequent (Fig. 4). Additionally, the soils horizons are moderately well defined (Fig. 4), suggesting minimal
341 cryoturbation.

342 Similar to Arena Valley and Wright Valley in the MDV (Graham et al., 2002; Schiller et al., 2009), NO_3^-
343 concentrations are highest just beneath the surface at Roberts Massif, indicating shallow salt migration under an arid
344 climate. These data indicate that the samples furthest inland at Roberts Massif and Thanksgiving Valley have been
345 fairly undisturbed since at least the middle to late Pleistocene, given the estimates of exposure duration (see Section
346 6.2). Since the meteoric ^{10}Be and NO_3^- profiles at Bennett Platform are mirrored, we argue that the difference could
347 be due to 1) additional ^{10}Be delivery or 2) enhanced NO_3^- transport. Bennett Platform was the only location we
348 sampled on a large moraine (Fig. 2c), and as a constructional landform we would expect ^{10}Be to be highest at the
349 surface and decrease to background concentrations. This is generally the observed behavior. The NO_3^- profile
350 behavior is similar to those throughout the Shackleton Glacier region, though the concentrations continue to increase
351 with depth, possibly indicating some percolation of NO_3^- rich brine. What may be considered the “anomalous” data
352 point is the surface concentration of meteoric ^{10}Be . Even though we sampled a constructional landform, the sample
353 was collected between two boulder lines in a small, local depression (~1 m) (Table 2). It is probably no coincidence

354 that this location also has the greatest proportion of fine-grained material in the soil profile. The two boulder lines
355 impede wind flow and act as a sediment and snow trap, possibly resulting in a higher concentration of meteoric ^{10}Be
356 than expected simply from atmospheric deposition. The snow in the depression may also aid in NO_3^- transport when
357 melted. In this case, additional sediment-laden ^{10}Be deposition (superseding any erosion) and/or possible salt
358 transport need to be considered to accurately date the moraine.

359 **6.2. Attempt at inferring surface exposure duration approximation and thoughts on glacial history**

360 We used the relationship between the maximum meteoric ^{10}Be concentration in the soil profile and the
361 meteoric ^{10}Be inventory (Graly et al., 2010) to speculatively infer ^{10}Be inventories and estimate maximum exposure
362 durations for all eleven locations with and without erosion using Eq. 5 (Fig. 7; Table 3). As is the case for Roberts
363 Massif and Thanksgiving Valley, the highest ^{10}Be concentrations may not always be at the surface for all locations;
364 however, the relationship is sufficiently strong to provide an estimate of the ^{10}Be inventory and thus an exposure
365 duration estimate.

$$366 \quad t = -\frac{1}{\lambda} \cdot \ln \left[1 - \frac{\lambda I}{Q - E\rho N} \right] \quad (5)$$

367 We did not measure erosion rates in this study. Balter-Kennedy et al. (2020) determined erosion rates for
368 boulders at Roberts Massif which were less than 2 cm Ma^{-1} . Considering we are investigating soils, we chose a
369 conservative value of 5 cm Ma^{-1} for our calculations. We selected a ^{10}Be flux value (Q) of $1.3 \times 10^5 \text{ atoms cm}^{-2} \text{ yr}^{-1}$
370 from Taylor Dome (Steig et al., 1995) due to a similar climate to that of the CTAM and an absence of local meteoric
371 ^{10}Be flux data.

372 Compared to the measured inventories from Roberts Massif, Bennett Platform, and Thanksgiving Valley
373 (from the ^{10}Be depth profiles; see Section 5.1), the inferred inventories differ by $\sim 16\text{-}130\%$. The inferred exposure
374 estimates with erosion range from 58 ka to $>6.5 \text{ Ma}$, and the estimates without erosion range from 57 ka to 1.94 Ma
375 for Mt. Speed and Roberts Massif, respectively (Fig 8; Table 3). With the exception of Roberts Massif,
376 Thanksgiving Valley, and Mt. Speed, the oldest surfaces are those which we sampled furthest from the glacier,
377 which is consistent with our sampling methodology to capture younger and older soils. The sample from Roberts
378 Massif collected closest to the glacier has an estimated exposure duration that is outside the model limits ($>6.5 \text{ Ma}$).

379 The youngest surfaces we sampled from the Shackleton Glacier region are those from the lowest elevations
380 and closest to the Ross Ice Shelf (Fig. 8). This is generally consistent with previous glacial modeling studies which
381 show that the greatest fluctuations in glacier height during the LGM were along outlet glacier and ice shelf margins
382 (Golledge et al., 2012; Mackintosh et al., 2011, 2014). Given the low erosion rates throughout Antarctica (Balter-
383 Kennedy et al., 2020; Ivy-Ochs et al., 1995; Morgan et al., 2010) and possibly low background concentrations of
384 meteoric ^{10}Be (Dickinson et al., 2012; Schiller et al., 2009; Valletta et al., 2015), the Mt. Speed, Mt. Wasko, and Mt.
385 Franke samples were all likely covered by Shackleton Glacier during the LGM, as well as the lower elevation, near-
386 glacier samples from Mt. Heekin, Bennett Platform, and Mt. Augustana. The soils from Schroeder Hill and Roberts
387 Massif have likely been exposed since the early Pleistocene (Fig. 8). We also attempted to estimate exposure
388 durations using two additional methods: 1) the measured ^{10}Be inventories for Roberts Massif, Bennett Platform, and
389 Thanksgiving Valley, and 2) by calculating ^{10}Be concentrations using regressions of NO_3^- and ^{10}Be for all seven
390 locations with depth profiles, as detailed in the supplementary materials. These exposure estimates are similar and
391 range from $\sim 100 \text{ ka}$ at Bennet Platform to $<4.5 \text{ Ma}$ at Roberts Massif (Fig. S4; Table S3).

392 Sirius Group deposits were observed at Roberts Massif and were deposited as Shackleton Glacier retreated
393 in this region (Fig. 2a). Evidence for a dynamic EAIS is derived primarily from the diamictite rocks (tills) of the
394 Sirius Group, which are found throughout the TAM and include well-documented outcrops in the Shackleton
395 Glacier region, but their age is unknown (Hambrey et al., 2003). Some of the deposits contain pieces of shrubby
396 vegetation, indicating that the Sirius Group formed under conditions warmer than present with woody plants
397 occupying inland portions of Antarctica (Webb et al., 1984, 1996; Webb and Harwood, 1991). Sparse marine

398 diatoms found in the sediments were initially interpreted as evidence for the formation of the Sirius Group via
399 glacial over riding of the TAM during the warmer Pliocene (Barrett et al., 1992), though it is now argued that the
400 marine diatoms were wind-derived contamination, indicating that the Sirius Group is older (Scherer et al., 2016;
401 Stroeven et al., 1996). We document a large diamictite at site RM2-8 that is underlain by soils with an inferred
402 exposure of at least 1.9 Ma, possibly greater than 6.5 Ma. These exposure duration estimates indicate that the loose
403 Sirius Group diamict was deposited at Roberts Massif some point after the Pliocene. While these data cannot
404 constrain the age of the formation, we suggest that the diamict could have formed prior to the Pliocene and was
405 transported during the Pleistocene glaciations.

406 **7. Conclusions**

407 We determined concentrations of meteoric ^{10}Be and NO_3^- in soils from eleven ice-free areas along
408 Shackleton Glacier, Antarctica, which are among the highest measured meteoric ^{10}Be concentrations from the polar
409 regions. Concentrations of meteoric ^{10}Be spanned from 1.9×10^8 atoms g^{-1} at Bennett Platform to 73×10^8 atoms g^{-1}
410 at Roberts Massif. The concentrations of NO_3^- were similarly variable and ranged from $\sim 1 \mu\text{g g}^{-1}$ near the ice shelf
411 to 15mg g^{-1} near the Polar Plateau. In general, the lowest concentrations of ^{10}Be and NO_3^- we measured were at low
412 elevations, near the ice shelf, and closest to the glacier.

413 Since NO_3^- and ^{10}Be are both derived from atmospheric deposition, we expect the shape of their
414 accumulation profiles to be similar at depth in hyper-arid soils. In general, this was true for Roberts Massif and
415 Thanksgiving Valley, while NO_3^- and ^{10}Be concentrations were mirrored at Bennett Platform. We conclude that
416 much of the southern Shackleton Glacier region has maintained persistent arid conditions since at least the
417 Pleistocene, though the region may have been warmer and wetter in the past, as evidenced by the presence of the
418 Sirius Group diamict. The onset of aridity is particularly important in understanding refugia and ecological
419 succession in TAM soils. Since the parts of the region have remained hyper-arid and undisturbed for upwards of a
420 few million years, prolonged exposure has resulted in the accumulation of salts at high concentrations in the soils. It
421 is an enigma how soil organisms have persisted throughout glacial-interglacial cycles. However, it is possible that
422 organisms have survived near the glacier at locations like Mt. Augustana, where glacial advance appears to have
423 been minimal during the LGM, but seasonal summer melt has the potential to solubilize salts.

424 Overall, our data show that the relatively youngest soils we sampled were at lower elevations near the
425 Shackleton Glacier terminus and lower elevations further inland (typically near the glacier). Inferred estimates range
426 from 57 ka (though likely post LGM when corrected) to 1.94 Ma, possibly >6.5 Ma with erosion. Our sampling
427 scheme was successful in capturing a range of surface exposure durations which can contribute to growing archives
428 in the CTAM. There are outstanding issues regarding inheritance dynamics of meteoric ^{10}Be in disturbed
429 environments, and particle erosion/deposition rates, and NO_3^- mobility. We hope that future studies will further
430 evaluate the relationship between water-soluble salts (e.g., NO_3^-) and meteoric ^{10}Be as a proxies for landscape
431 disturbance and exposure age.

432

433 **Author Contributions**

434 The project was designed and funded by BJA, DHW, IDH, NF, and WBL. Fieldwork was conducted by BJA, DHW,
435 IDH, NF, and MAD. LBC, PRB, and MAD prepared the samples for meteoric ^{10}Be analysis and MAD analyzed the
436 samples for NO_3^- . MAD wrote the article with contributions and edits from all authors.

437 **Data Availability Statement**

438 The datasets generated for this study are included in the article or supplementary materials.

439 **Competing Interests**

440 The authors declare that they have no conflict of interest.

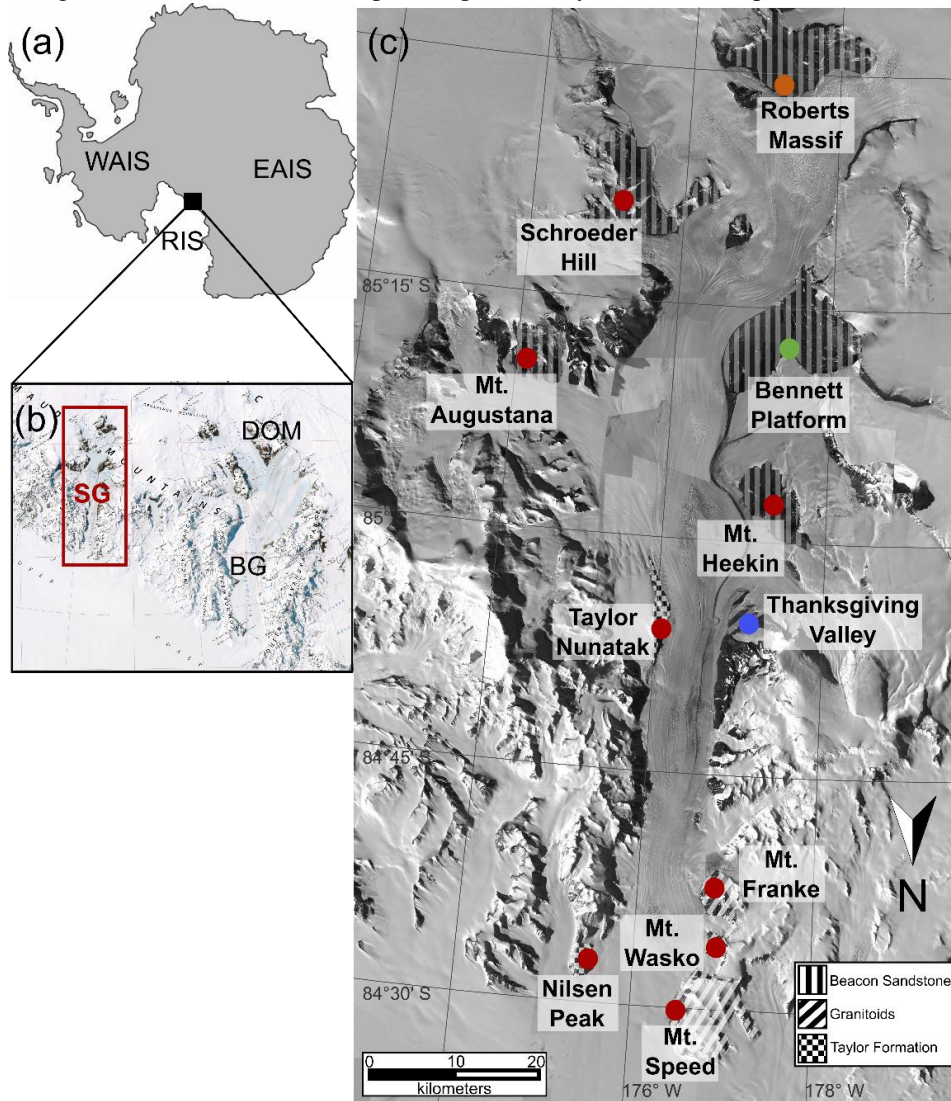
441 **Acknowledgments**

442 We thank the United States Antarctic Program (USAP), Antarctic Science Contractors (ASC), Petroleum
443 Helicopters Inc. (PHI), and Marci Shaver-Adams for logistical and field support. We especially thank Dr. Marc
444 Caffee and the Purdue University PRIME Lab for their assistance with AMS measurements. Additionally, we thank
445 Dr. Andrew Christ at University of Vermont for thoughtful discussions and Dr. Sue Welch and Daniel Gilbert at The
446 Ohio State University for help with initial laboratory analyses. We appreciate the detailed and thoughtful
447 suggestions and edits from Dr. Brent Goehring and an anonymous reviewer which have greatly improved this
448 manuscript. This work was supported by NSF OPP grants 1341631 (WBL), 1341618 (DHW), 1341629 (NF),
449 1341736 (BJA), NSF-DGE 1840280 (GRFP) (MAD), and a PRIME Lab seed proposal (MAD). Sample preparation
450 and LBC's time supported by NSF EAR 1735676. Geospatial support for this work provided by the Polar Geospatial
451 Center under NSF OPP grants 1043681 and 1559691.

452

453 **Figures:**

454 **Figure 1:** Outline map of the Antarctic continent (a), the Shackleton Glacier (SG) and Beardmore Glacier (BG)
455 regions (b), and an overview map of Shackleton Glacier (c). The red box in (b) encapsulates the Shackleton Glacier
456 region. The red circles in (c) represent our eleven sampling locations, with an emphasis on Roberts Massif (orange),
457 Bennett Platform (green), and Thanksgiving Valley (blue), which have the most comprehensive dataset in this study.
458 The bedrock serves as primary weathering product for soil formation (Elliot and Fanning, 2008; Paulsen et al.,
459 2004). For reference, the East Antarctic Ice Sheet (EAIS), West Antarctic Ice Sheet (WAIS), Ross Ice Shelf (RIS),
460 and Dominion Range are labeled (a, b). Base maps were provided by the Polar Geospatial Center.



461

462

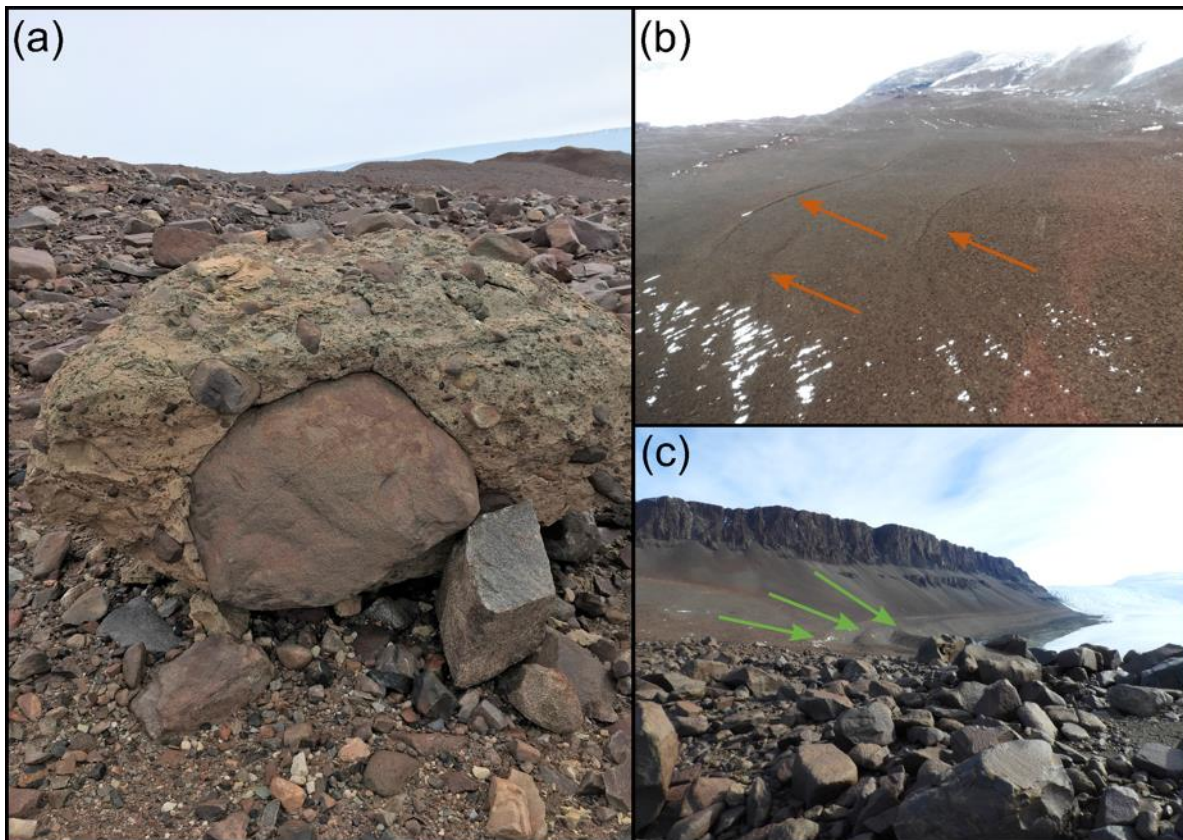
463

464

465

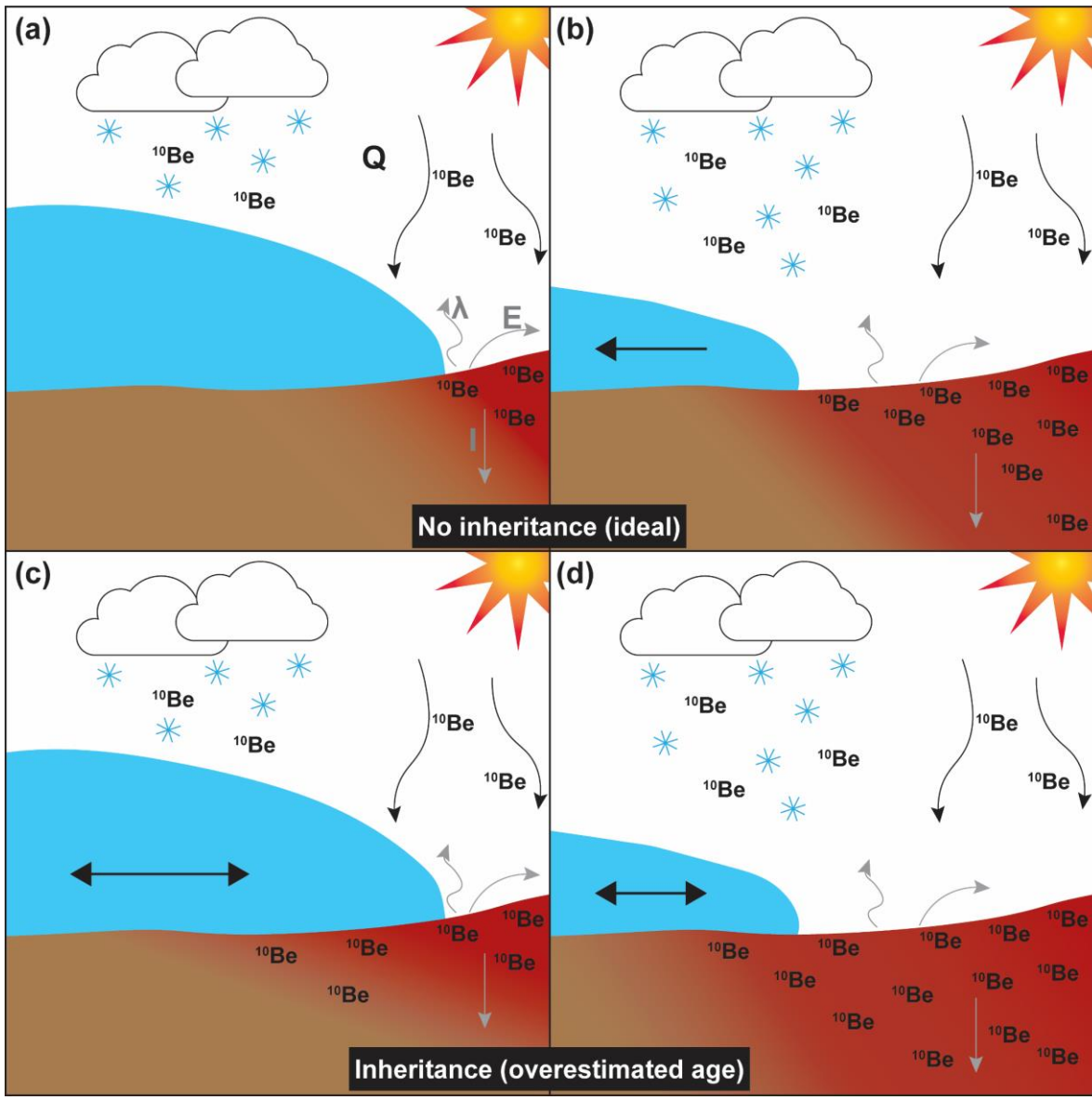
466

Figure 2: The Sirius Group was documented at Roberts Massif near the RM2-8 sampling location (a). Small moraines were observed at Roberts Massif (b) and large moraines at Bennett Platform (c).



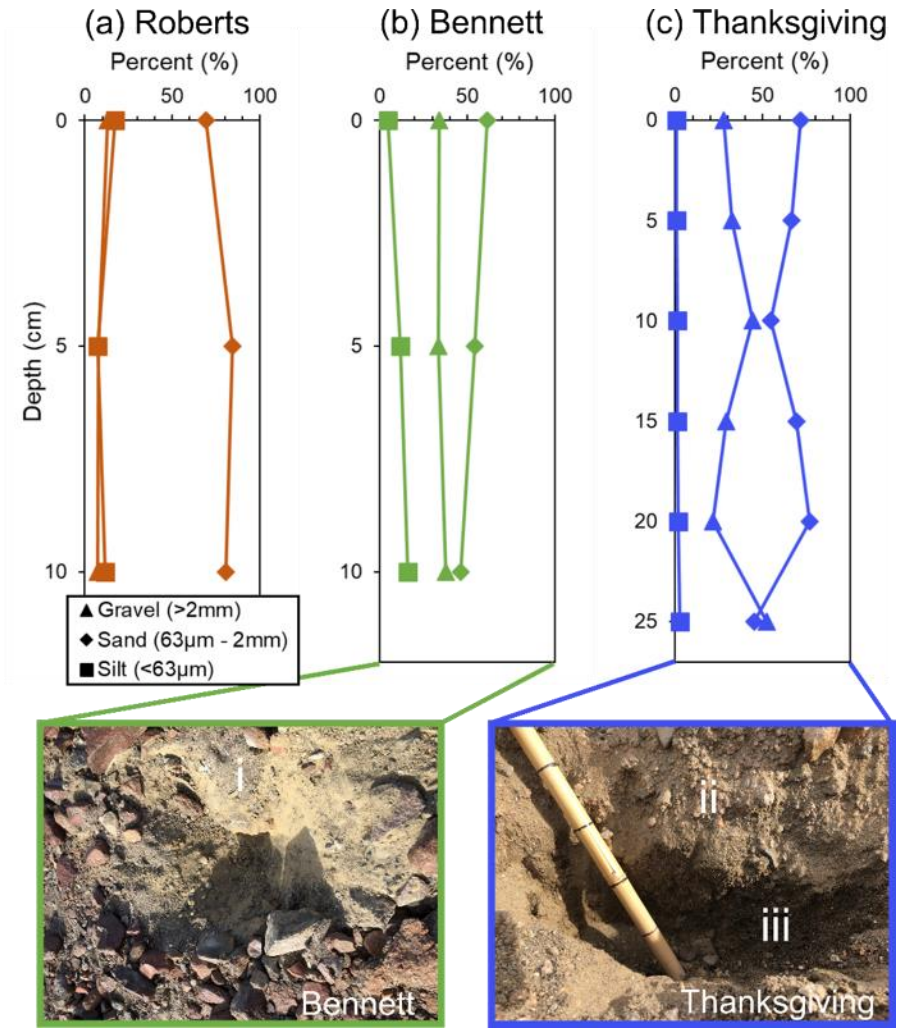
467

468 **Figure 3:** Conceptual diagram of meteoric ^{10}Be accumulation in soils during glacial advance and retreat. In “ideal”
 469 conditions, ^{10}Be accumulates in exposed soils by wet deposition (with snow) and dry deposition (by gravity as
 470 indicated by black arrows) and ^{10}Be concentrations beneath the glacier are negligible at background levels (a). As
 471 the glacier retreats, ^{10}Be can begin accumulating in the recently exposed soil and an inventory can be measured to
 472 calculate exposure duration. In the case where the glacier has waxed and waned numerous times and the soils
 473 already contain a non-negligible “inheritance” concentration of ^{10}Be , the inventories would need to be corrected for
 474 ^{10}Be inheritance (c-d) to accurately determine exposure duration. Q represents of the flux of ^{10}Be to the surface, λ
 475 represents radioactive decay of ^{10}Be , E represents erosion, and I represents the migration of ^{10}Be from the surface to
 476 depth.
 477



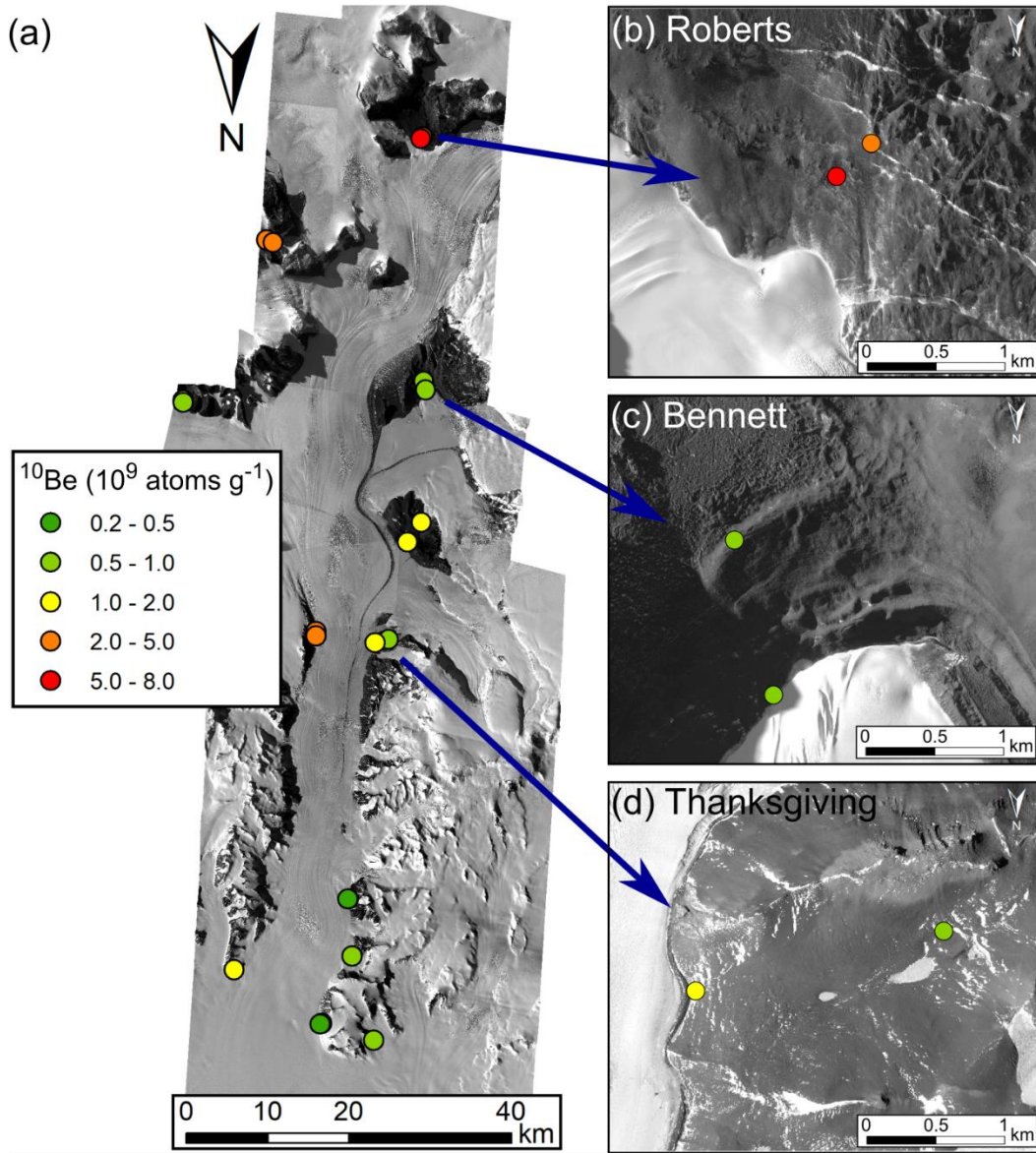
478

479 **Figure 4:** The grain size composition of soil profiles collected from Roberts Massif (a, orange), Bennett Platform (b, green),
 480 and Thanksgiving Valley (c, blue). The soil pits from Bennett Platform and Thanksgiving Valley are also
 481 shown with distinct soil horizons. The different soil horizons observed at Bennett Platform and Thanksgiving Valley
 482 are indicated by i, ii, and iii.
 483



484

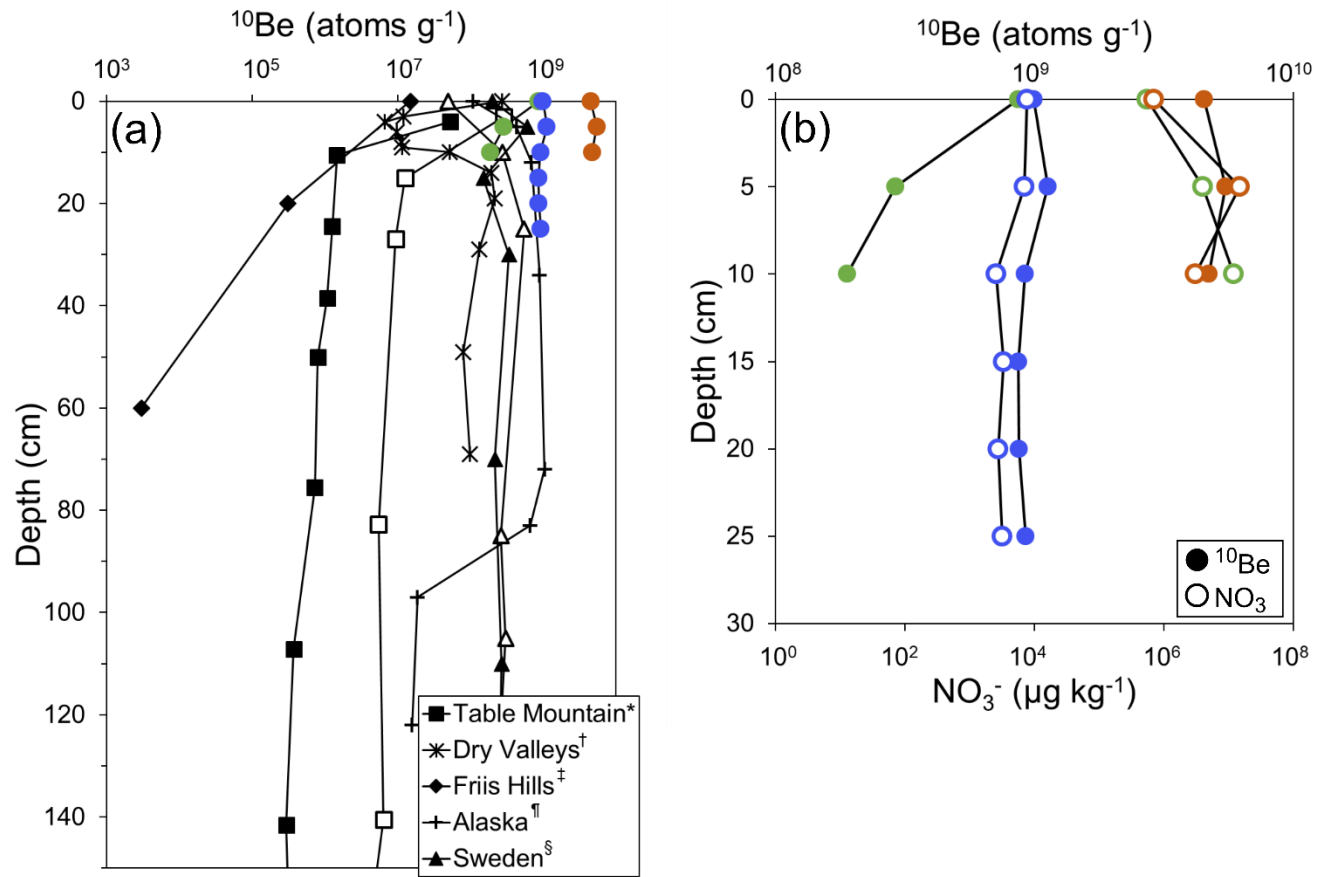
485 **Figure 5:** Spatial distribution of surface meteoric ^{10}Be concentrations in the Shackleton Glacier region (a). Where
 486 possible, two samples were collected at each location to represent surfaces closest to the glacier, which might have
 487 been glaciated during recent glacial periods, and samples furthest from the glacier that are likely to have been
 488 exposed during recent glacial periods. Insets of Roberts Massif (b), Bennett Platform (c), and Thanksgiving Valley
 489 (d) are included, as these locations have both ^{10}Be and NO_3^- depth profile data. Base maps were provided by the
 490 Polar Geospatial Center.
 491



492

493 **Figure 6:** Soil profiles of meteoric ^{10}Be concentrations for Roberts Massif (orange), Bennett Platform (green), and
 494 Thanksgiving Valley (blue) compared to profiles from the Antarctic (Dickinson et al., 2012^{*}; Schiller et al., 2009[†];
 495 Valletta et al., 2015[‡]) and Arctic (Bierman et al., 2014[¶]; Ebert et al., 2012[§]) (a). The ^{10}Be concentration profiles were
 496 also compared to NO_3^- concentration profiles (b).
 497

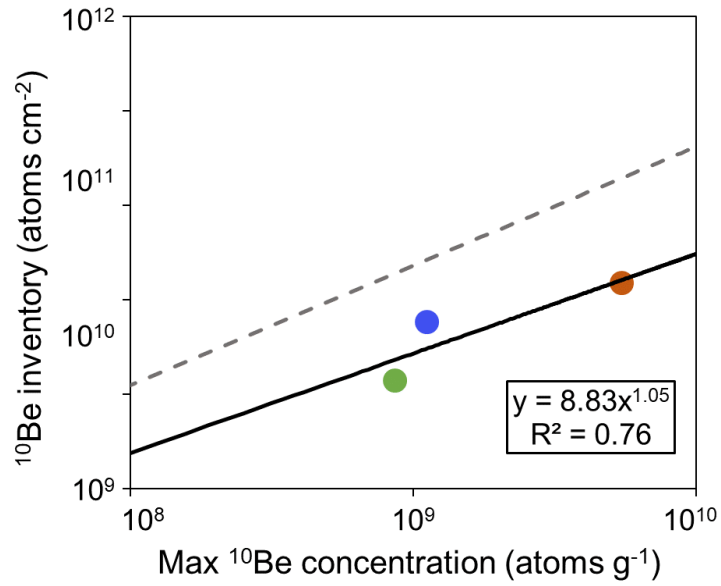
498



499

500

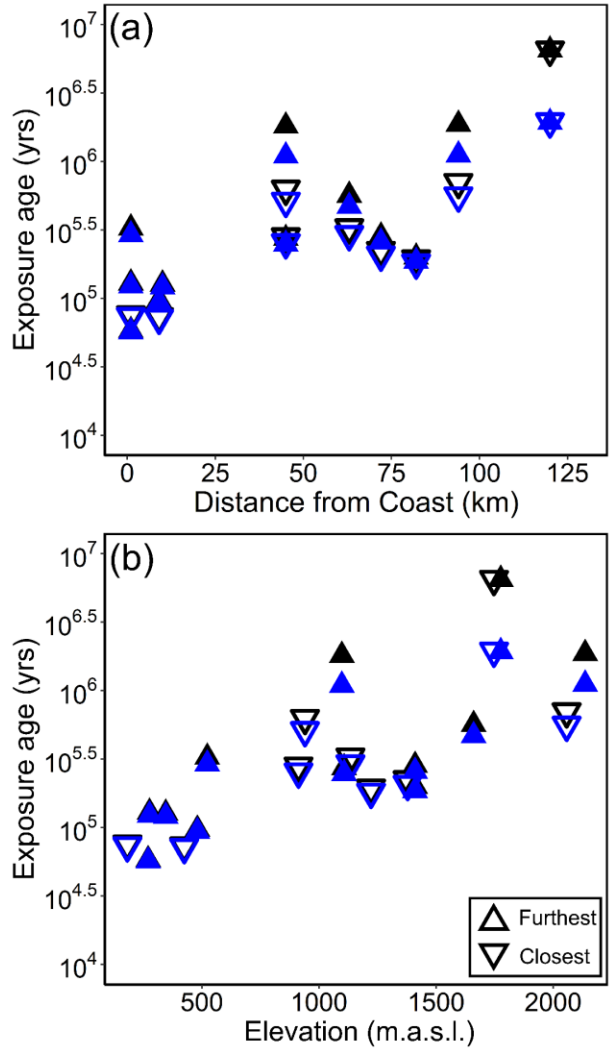
501 **Figure 7:** Relationship between the measured maximum (or surface) meteoric ^{10}Be concentration and the calculated
502 inventory (Eq. 2). This relationship is used to infer ^{10}Be inventories given a maximum or surface concentration
503 (Graly et al., 2010). The solid black line is the power relationship between concentration and inventory, while the
504 dashed grey line is the regression from Graly et al. (2010).
505



506

507

508 **Figure 8:** Inferred surface exposure durations versus distance from the coast (a) and elevation (b), with (black) and
509 without (blue) an assumed erosion term. Upward facing triangles are samples collected furthest from the glacier,
510 while downward triangles are samples collected closest to the glacier.



511

512 **Table 1:** Concentrations of meteoric ^{10}Be and water-soluble nitrate (NO_3^-) in Shackleton Glacier region surface soils and depth profiles. Additional information
 513 on ^{10}Be corrections is located in Table S2.
 514

Sample Name	Location	Latitude	Longitude	Elevation (m.a.s.l.)	Distance from Coast (km)	Depth (cm)	^{10}Be Concentration (10^9 atoms g^{-1})	NO_3^- Concentration (10^5 $\mu\text{g kg}^{-1}$)
AV2-1	Mt. Augustana	-85.1706	-174.1338	1410	72	0-5	1.162	7.77
AV2-1	Mt. Augustana	-85.1706	-174.1338	1410	72	5-10	-	12.2
AV2-1	Mt. Augustana	-85.1706	-174.1338	1410	72	10-15	-	13.4
AV2-8	Mt. Augustana	-85.1676	-174.1393	1378	72	0-5	0.955	-
BP2-1	Bennett Platform	-85.2121	-177.3576	1410	82	0-5	0.868	5.57
BP2-1	Bennett Platform	-85.2121	-177.3576	1410	82	5-10	0.291	39.8
BP2-1	Bennett Platform	-85.2121	-177.3576	1410	82	10-15	0.188	121
BP2-8	Bennett Platform	-85.2024	-177.3907	1222	82	0-5	0.848	-
MF2-1	Mt. Franke	-84.6236	-176.7353	480	9	0-5	0.462	0.041
MF2-1	Mt. Franke	-84.6236	-176.7353	480	9	5-10	-	0.014
MF2-1	Mt. Franke	-84.6236	-176.7353	480	9	10-15	-	0.010
MF2-1	Mt. Franke	-84.6236	-176.7353	480	9	15-20	-	0.011
MF2-4	Mt. Franke	-84.6237	-176.7252	424	9	0-5	0.360	-
MH2-1	Mt. Heekin	-85.0299	-177.2405	1098	63	0-5	1.956	18.0
MH2-1	Mt. Heekin	-85.0299	-177.2405	1098	63	5-10	-	27.4
MH2-1	Mt. Heekin	-85.0299	-177.2405	1098	63	10-15	-	18.8
MH2-8	Mt. Heekin	-85.0528	-177.4099	1209	63	0-5	1.300	-
MSP2-1	Mt. Speed	-84.4819	-176.5070	270	0	0-5	0.291	-
MSP2-4	Mt. Speed	-84.4811	-176.4864	181	0	0-5	0.370	-
MSP4-1	Mt. Speed	-84.4661	-177.1224	276	0	0-5	0.596	-
MW4-1	Mt. Wasko	-84.5600	-176.8177	345	10	0-5	0.586	-
NP2-5	Nilsen Peak	-84.6227	-176.7501	522	0	0-5	1.295	-
RM2-1	Roberts Massif	-85.4879	-177.1844	1776	120	0-5	4.538	6.94
RM2-1	Roberts Massif	-85.4879	-177.1844	1776	120	5-10	5.475	149
RM2-1	Roberts Massif	-85.4879	-177.1844	1776	120	10-15	4.721	30.7
RM2-8	Roberts Massif	-85.4857	-177.1549	1747	120	0-5	7.327	-
SH3-2	Schroeder Hill	-85.3597	-175.0693	2137	94	0-5	3.850	75.5
SH3-2	Schroeder Hill	-85.3597	-175.0693	2137	94	5-10	-	16.1

SH3-2	Schroeder Hill	-85.3597	-175.0693	2137	94	10-15	-	41.6
SH3-8	Schroeder Hill	-85.3569	-175.1621	2057	94	0-5	2.267	-
TGV2-1	Thanksgiving Valley	-84.9190	-177.0603	1107	45	0-5	0.993	0.077
TGV2-1	Thanksgiving Valley	-84.9190	-177.0603	1107	45	5-10	1.125	0.071
TGV2-1	Thanksgiving Valley	-84.9190	-177.0603	1107	45	10-15	0.921	0.025
TGV2-1	Thanksgiving Valley	-84.9190	-177.0603	1107	45	15-20	0.864	0.033
TGV2-1	Thanksgiving Valley	-84.9190	-177.0603	1107	45	20-25	0.874	0.028
TGV2-1	Thanksgiving Valley	-84.9190	-177.0603	1107	45	25-30	0.925	0.031
TGV2-8	Thanksgiving Valley	-84.9145	-176.8860	912	45	0-5	1.152	-
TN3-1	Taylor Nunatak	-84.9227	-176.1242	1097	45	0-5	3.802	-
TN3-5	Taylor Nunatak	-84.9182	-176.1282	940	45	0-5	2.105	

515

516
517

Table 2: Surface features of the sample locations from the Shackleton Glacier region.

Location	Sample name	Sample description
Mt. Augustana	AV2-1	Up valley from Gallup Glacier (tributary glacier); at valley floor; surface covered by cobbles and pebbles; red-stained sandstones nearby; frozen ground at bottom of depth profile
Mt. Augustana	AV2-8	At toe of Gallup Glacier; surface covered primarily by boulders; mainly sand between boulders
Bennett Platform	BP2-1	On larger moraine; local depression between two boulder lines, up valley from McGregor Glacier (tributary glacier); at valley floor
Bennett Platform	BP2-8	At toe of McGregor Glacier (tributary glacier); surface covered primarily by boulders; mainly sand between boulders
Mt. Franke	MF2-1	Bottom of wide valley floor; near small moraine; frozen soil at bottom of depth profile
Mt. Franke	MF2-4	Bottom of wide valley floor; near small moraine
Mt. Heekin	MH2-1	On high-elevation saddle; surface covered by sparse small boulders, cobbles, and pebbles; poorly consolidated till; frozen ground at bottom of profile
Mt. Heekin	MH2-8	At toe of Baldwin Glacier (alpine glacier) on valley floor; two ponds nearby; surface covered by loose rocks and sand; poorly consolidated till; possible polygonal surface nearby
Mt. Speed	MSP2-1	Steep slope; large granite boulders; scree
Mt. Speed	MSP2-4	Near cliff by Shackleton Glacier; large granite boulders; scree
Mt. Speed	MSP4-1	Spur on level with glacier; frozen soil near 5 cm depth
Mt. Wasko	MW4-1	Steep slope; large granite boulders; scree; nearby snowpack
Nilsen Peak	NP2-5	On ridge; near large snow patch
Roberts Massif	RM2-1	Near thin moraine; red-stained sandstones nearby with etches; frozen ground at bottom of depth profile
Roberts Massif	RM2-8	Near thin moraine and Sirius Group diamict; large boulders nearby with unconsolidated sediment
Schroeder Hill	SH3-2	Red-stained sandstone; poorly consolidated till; bedrock at bottom of profile
Schroeder Hill	SH3-8	Red-stained sandstone; poorly consolidated till
Thanksgiving Valley	TGV2-1	Slightly uphill on valley wall; poorly consolidated till; frozen ground at bottom of depth profile; polygonal surface nearby
Thanksgiving Valley	TGV2-8	At the toe of Shackleton Glacier; near thin moraines; surface covered primarily by large boulders
Taylor Nunatak	TN3-1	On ridge; surface covered by small boulders with underlying silt; frozen ground at bottom of depth profile
Taylor Nunatak	TN3-5	Valley floor; nearby snow patches; few glacial erratics; surface covered primarily by small boulders and cobbles with underlying silt

518
519
520

521
522
523

Table 3: Estimated exposure durations using relationship between maximum ¹⁰Be concentration and the calculated inventory, see Figure 7 (Graly et al., 2010).

Sample name	Measured inventory (10 ¹¹ atoms)	Inferred inventory (10 ¹¹ atoms)	Inferred exposure duration with <i>E</i> (Ma)	Inferred exposure duration without <i>E</i> (Ma)
AV2-1		0.38	0.285	0.258
AV2-8		0.33	0.224	0.207
BP2-1	0.135	0.31	0.200	0.186
BP2-8		0.31	0.195	0.181
MF2-1		0.21	0.097	0.094
MF2-4		0.18	0.074	0.072
MH2-1		0.59	0.565	0.469
MH2-8		0.42	0.328	0.292
MSP2-1		0.16	0.058	0.057
MSP2-4		0.18	0.076	0.074
MSP4-1		0.24	0.129	0.123
MW4-1		0.24	0.127	0.121
NP2-5		0.42	0.326	0.291
RM2-1	1.47	1.24	>6.5*	1.93
RM2-8		1.50	>6.5*	1.94
SH3-2		1.07	1.87	1.11
SH3-8		0.67	0.702	0.560
TGV2-1	0.535	0.34	0.274	0.248
TGV2-8		0.38	0.282	0.255
TN3-1		1.06	1.81	1.09
TN3-5		0.62	0.628	0.512
*Outside of model range				

524
525

- 526 **References**
527 Ackert, R. P. and Kurz, M. D.: Age and uplift rates of Sirius Group sediments in the Dominion Range, Antarctica,
528 from surface exposure dating and geomorphology, *Glob. Planet. Change*, 42(1–4), 207–225,
529 doi:10.1016/j.gloplacha.2004.02.001, 2004.
- 530 Anderson, J. B., Shipp, S. S., Lowe, A. L., Wellner, J. S. and Mosola, A. B.: The Antarctic Ice Sheet during the Last
531 Glacial Maximum and its subsequent retreat history: a review, *Quat. Sci. Rev.*, 21, 49–70, doi:10.1016/S0277-
532 3791(01)00083-X, 2002.
- 533 Augustin, L., Barbante, C., Barnes, P. R. F., Barnola, J. M., Bigler, M., Castellano, E., Cattani, O., Chappellaz, J.,
534 Dahl-Jensen, D., Delmonte, B., Dreyfus, G., Durand, G., Falourd, S., Fischer, H., Flückiger, J., Hansson, M. E.,
535 Huybrechts, P., Jugie, G., Johnsen, S. J., Jouzel, J., Kaufmann, P., Kipfstuhl, J., Lambert, F., Lipenkov, V. Y., Littot,
536 G. C., Longinelli, A., Lorrain, R., Maggi, V., Masson-Delmotte, V., Miller, H., Mulvaney, R., Oerlemans, J., Oerter,
537 H., Orombelli, G., Parrenin, F., Peel, D. A., Petit, J. R., Raynaud, D., Ritz, C., Ruth, U., Schwander, J., Siegenthaler,
538 U., Souchez, R., Stauffer, B., Steffensen, J. P., Stenni, B., Stocker, T. F., Tabacco, I. E., Udisti, R., van de Wal, R. S.
539 W., van den Broeke, M., Weiss, J., Wilhelms, F., Winther, J. G., Wolff, E. W. and Zucchelli, M.: Eight glacial
540 cycles from an Antarctic ice core, *Nature*, 429(6992), 623–628, doi:10.1038/nature02599, 2004.
- 541 Balter-Kennedy, A., Bromley, G., Balco, G., Thomas, H. and Jackson, M. S.: A 14.5-million-year record of East
542 Antarctic Ice Sheet fluctuations from the central Transantarctic Mountains, constrained with cosmogenic ³He, ¹⁰Be,
543 ²¹Ne, and ²⁶Al, *Cryosph.*, 14(8), 2647–2672, doi:10.5194/tc-2020-57, 2020.
- 544 Barrett, P. J.: Resolving views on Antarctic Neogene glacial history - The Sirius debate, *Earth Environ. Sci. Trans.*
545 *R. Soc. Edinburgh*, 104(1), 31–53, doi:10.1017/S175569101300008X, 2013.
- 546 Barrett, P. J., Adams, C. J., McIntosh, W. C., Swisher, C. C. and Wilson, G. S.: Geochronological evidence
547 supporting Antarctic deglaciation three million years ago, *Nature*, 359, 816–818, 1992.
- 548 Bierman, P. R., Corbett, L. B., Graly, J. A., Neumann, T. A., Lini, A., Crosby, B. T. and Rood, D. H.: Preservation
549 of a Preglacial Landscape Under the Center of the Greenland Ice Sheet, *Science* (80-.), 344, 402–405,
550 doi:10.4159/harvard.9780674430501.c21, 2014.
- 551 Bockheim, J. G.: Landform and Soil Development in the McMurdo Dry Valleys, Antarctica: A Regional Synthesis,
552 *Arctic, Antarct. Alp. Res.*, 34(3), 308–317, doi:10.1080/15230430.2002.12003499, 2002.
- 553 Bromley, G. R. M., Hall, B. L., Stone, J. O., Conway, H. and Todd, C. E.: Late Cenozoic deposits at Reedy Glacier,
554 Transantarctic Mountains: implications for former thickness of the West Antarctic Ice Sheet, *Quat. Sci. Rev.*, 29(3–
555 4), 384–398, doi:10.1016/j.quascirev.2009.07.001, 2010.
- 556 Brown, E. T., Edmond, J. M., Raisbeck, G. M., Bournès, D. L., Yiou, F. and Measures, C. I.: Beryllium isotope
557 geochemistry in tropical river basins, *Geochim. Cosmochim. Acta*, 56(4), 1607–1624, doi:10.1016/0016-
558 7037(92)90228-B, 1992.
- 559 Cary, S. C., McDonald, I. R., Barrett, J. E. and Cowan, D. A.: On the rocks: The microbiology of Antarctic Dry
560 Valley soils, *Nat. Rev. Microbiol.*, 8(2), 129–138, doi:10.1038/nrmicro2281, 2010.
- 561 Claridge, G. G. C. and Campbell, I. B.: Origin of nitrate deposits., 1968a.
- 562 Claridge, G. G. C. and Campbell, I. B.: Soils of the Shackleton glacier region, Queen Maud Range, Antarctica, *New*
563 *Zeal. J. Sci.*, 11(2), 171–218, 1968b.
- 564 Claridge, G. G. C. and Campbell, I. B.: Salts in Antarctic soils, their distribution and relationship to soil processes,
565 *Soil Sci.*, 123(6), 377–384, 1977.
- 566 Clark, P. U., Dyke, A. S., Shakun, J. D., Carlson, A. E., Clark, J., Wohlfarth, B., Mitrovica, J. X., Hostetler, S. W.
567 and McCabe, A. M.: The Last Glacial Maximum, *Science* (80-.), 325, 710–714, doi:10.1126/science.1172873,
568 2009.
- 569 Collins, G. E., Hogg, I. D., Convey, P., Sancho, L. G., Cowan, D. A., Lyons, W. B., Adams, B. J., Wall, D. H. and
570 Green, T. G. A.: Genetic diversity of soil invertebrates corroborates timing estimates for past collapses of the West

- 571 Antarctic Ice Sheet, *Proc. Natl. Acad. Sci. U. S. A.*, 117(36), 22293–22302, doi:10.1073/pnas.2007925117, 2020.
- 572 Convey, P., Gibson, J. A. E., Hillenbrand, C. D., Hodgson, D. A., Pugh, P. J. A., Smellie, J. L. and Stevens, M. I.:
573 Antarctic terrestrial life - Challenging the history of the frozen continent?, *Biol. Rev.*, 83(2), 103–117,
574 doi:10.1111/j.1469-185X.2008.00034.x, 2008.
- 575 Diaz, M. A., Li, J., Michalski, G., Darrah, T. H., Adams, B. J., Wall, D. H., Hogg, I. D., Fierer, N., Welch, S. A.,
576 Gardner, C. B. and Lyons, W. B.: Stable isotopes of nitrate, sulfate, and carbonate in soils from the Transantarctic
577 Mountains, Antarctica: A record of atmospheric deposition and chemical weathering, *Front. Earth Sci.*, 8(341),
578 doi:10.3389/feart.2020.00341, 2020.
- 579 Dickinson, W. W., Schiller, M., Ditchburn, B. G., Graham, I. J. and Zondervan, A.: Meteoric Be-10 from Sirius
580 Group suggests high elevation McMurdo Dry Valleys permanently frozen since 6 Ma, *Earth Planet. Sci. Lett.*, 355–
581 356, 13–19, doi:10.1016/j.epsl.2012.09.003, 2012.
- 582 Ebert, K., Willenbring, J., Norton, K. P., Hall, A. and Hättestrand, C.: Meteoric ¹⁰Be concentrations from saprolite
583 and till in northern Sweden: Implications for glacial erosion and age, *Quat. Geochronol.*, 12, 11–22,
584 doi:10.1016/j.quageo.2012.05.005, 2012.
- 585 Elliot, D. H. and Fanning, C. M.: Detrital zircons from upper Permian and lower Triassic Victoria Group sandstones,
586 Shackleton Glacier region, Antarctica: Evidence for multiple sources along the Gondwana plate margin, *Gondwana
587 Res.*, 13, 259–274, doi:10.1016/j.gr.2007.05.003, 2008.
- 588 Elliot, D. H., Collinson, J. W. and Green, W. J.: Lakes in dry valleys at 85°S near Mount Heekin, Shackleton
589 Glacier, *Antarct. J. United States*, 31(2), 25–27, 1996.
- 590 Everett, K. R.: SOILS OF THE MESERVE GLACIER AREA, WRIGHT VALLEY, SOUTH VICTORIA LAND,
591 ANTARCTICA, *Soil Sci.*, 112(6), 425–438 [online] Available from: [https://oae.ovid.com/article/00010694-
592 197112000-00007/HTML](https://oae.ovid.com/article/00010694-197112000-00007/HTML) (Accessed 17 June 2021), 1971.
- 593 Fraser, C. I., Nikula, R., Ruzzante, D. E. and Waters, J. M.: Poleward bound: Biological impacts of Southern
594 Hemisphere glaciation, *Trends Ecol. Evol.*, 27(8), 462–471, doi:10.1016/j.tree.2012.04.011, 2012.
- 595 Frey, M. M., Savarino, J., Morin, S., Erbland, J. and Martins, J. M. F.: Photolysis imprint in the nitrate stable isotope
596 signal in snow and atmosphere of East Antarctica and implications for reactive nitrogen cycling., 2009.
- 597 Gasson, E., DeConto, R. M., Pollard, D. and Levy, R. H.: Dynamic Antarctic ice sheet during the early to mid-
598 Miocene, *Proc. Natl. Acad. Sci. U. S. A.*, 113(13), 3459–3464, doi:10.1073/pnas.1516130113, 2016.
- 599 Golledge, N. R., Fogwill, C. J., Mackintosh, A. N. and Buckley, K. M.: Dynamics of the last glacial maximum
600 Antarctic ice-sheet and its response to ocean forcing, *Proc. Natl. Acad. Sci. U. S. A.*, 109(40), 16052–16056,
601 doi:10.1073/pnas.1205385109, 2012.
- 602 Golledge, N. R., Levy, R. H., McKay, R. M., Fogwill, C. J., White, D. A., Graham, A. G. C., Smith, J. A.,
603 Hillenbrand, C. D., Licht, K. J., Denton, G. H., Ackert, R. P., Maas, S. M. and Hall, B. L.: Glaciology and
604 geological signature of the Last Glacial Maximum Antarctic ice sheet, *Quat. Sci. Rev.*, 78, 225–247,
605 doi:10.1016/j.quascirev.2013.08.011, 2013.
- 606 Graham, I., Ditchburn, R. G., Claridge, G. G. G., Whitehead, N. E., Zondervan, A. and Sheppard, D. S.: Dating
607 Antarctic soils using atmospheric derived ¹⁰Be and nitrate, *R. Soc. New Zeal. Bull.*, 35, 429–436, 2002.
- 608 Graham, I. J., Ditchburn, R. G., Sparks, R. J. and Whitehead, N. E.: ¹⁰Be investigations of sediments, soils and loess
609 at GNS, *Nucl. Instruments Methods Phys. Res. B*, 123, 307–318, 1997.
- 610 Graly, J. A., Bierman, P. R., Reusser, L. J. and Pavich, M. J.: Meteoric ¹⁰Be in soil profiles - A global meta-
611 analysis, *Geochim. Cosmochim. Acta*, 74, 6814–6829, doi:10.1016/j.gca.2010.08.036, 2010.
- 612 Graly, J. A., Licht, K. J., Druschel, G. K. and Kaplan, M. R.: Polar desert chronologies through quantitative
613 measurements of salt accumulation, *Geology*, 46(4), 351–354, doi:10.1130/G39650.1, 2018.
- 614 Gulick, S. P. S., Shevenell, A. E., Montelli, A., Fernandez, R., Smith, C., Warny, S., Bohaty, S. M., Sjunneskog, C.,

- 615 Leventer, A., Frederick, B. and Blankenship, D. D.: Initiation and long-term instability of the East Antarctic Ice
616 Sheet, *Nature*, 552(7684), 225–229, doi:10.1038/nature25026, 2017.
- 617 Hambrey, M. J., Webb, P. N., Harwood, D. M. and Krissek, L. A.: Neogene glacial record from the Sirius Group of
618 the Shackleton Glacier region, central Transantarctic Mountains, Antarctica, *GSA Bull.*, 115(8), 994–1015,
619 doi:10.1130/B25183.1, 2003.
- 620 Ivy-Ochs, S., Schluchter, C., Kubik, P. W., Dittrich-Hannen, B. and Beer, J.: Minimum ¹⁰Be exposure ages of early
621 Pliocene for the Table Mountain plateau and the Sirius Group at Mount Fleming, Dry Valleys, Antarctica, *Geology*,
622 23(11), 1007–1010, 1995.
- 623 Jackson, A., Davila, A. F., Böhlke, J. K., Sturchio, N. C., Sevanthi, R., Estrada, N., Brundrett, M., Lacelle, D.,
624 McKay, C. P., Poghosyan, A., Pollard, W. and Zacny, K.: Deposition, accumulation, and alteration of Cl⁻, NO₃⁻,
625 ClO₄⁻ and ClO₃⁻ salts in a hyper-arid polar environment: Mass balance and isotopic constraints, *Geochim.*
626 *Cosmochim. Acta*, 182, 197–215, doi:10.1016/j.gca.2016.03.012, 2016.
- 627 Jones, R. S., Mackintosh, A. N., Norton, K. P., Golledge, N. R., Fogwill, C. J., Kubik, P. W., Christl, M. and
628 Greenwood, S. L.: Rapid Holocene thinning of an East Antarctic outlet glacier driven by marine ice sheet instability,
629 *Nat. Commun.*, 6(8910), 9910, doi:10.1038/ncomms9910, 2015.
- 630 Kaplan, M. R., Licht, K. J., Winckler, G., Schaefer, J. M., Bader, N., Mathieson, C., Roberts, M., Kassab, C. M.,
631 Schwartz, R. and Graly, J. A.: Middle to Late Pleistocene stability of the central East Antarctic Ice Sheet at the head
632 of Law Glacier, *Geology*, 45(11), 963–966, doi:10.1130/G39189.1, 2017.
- 633 Korschinek, G., Bergmaier, A., Faestermann, T., Gerstmann, U. C., Knie, K., Rugel, G., Wallner, A., Dillmann, I.,
634 Dollinger, G., von Gostomski, C. L., Kossert, K., Maiti, M., Poutivtsev, M. and Remmert, A.: A new value for the
635 half-life of ¹⁰Be by Heavy-Ion Elastic Recoil Detection and liquid scintillation counting, *Nucl. Instruments*
636 *Methods Phys. Res. Sect. B Beam Interact. with Mater. Atoms*, 268(2), 187–191, doi:10.1016/j.nimb.2009.09.020,
637 2010.
- 638 Lewis, A. R., Marchant, D. R., Ashworth, A. C., Hedenäs, L., Hemming, S. R., Johnson, J. V., Leng, M. J.,
639 Machlus, M. L., Newton, A. E., Raine, J. I., Willenbring, J. K., Williams, M. and Wolfe, A. P.: Mid-Miocene
640 cooling and the extinction of tundra in continental Antarctica, *Proc. Natl. Acad. Sci. U. S. A.*, 105(31), 10676–
641 10680, doi:10.1073/pnas.0802501105, 2008.
- 642 Lyons, W. B., Mayewski, P. A., Spencer, M. J. and Twickler, M. S.: Nitrate concentrations in snow from remote
643 areas: implication for the global NO_x flux, *Biogeochemistry*, 9(3), 211–222, doi:10.1007/BF00000599, 1990.
- 644 Lyons, W. B., Deuerling, K., Welch, K. A., Welch, S. A., Michalski, G., Walters, W. W., Nielsen, U., Wall, D. H.,
645 Hogg, I. and Adams, B. J.: The Soil Geochemistry in the Beardmore Glacier Region, Antarctica: Implications for
646 Terrestrial Ecosystem History, *Sci. Rep.*, 6, 26189, doi:10.1038/srep26189, 2016.
- 647 Mackintosh, A., Golledge, N., Domack, E., Dunbar, R., Leventer, A., White, D., Pollard, D., Deconto, R., Fink, D.,
648 Zwartz, D., Gore, D. and Lavoie, C.: Retreat of the East Antarctic ice sheet during the last glacial termination, *Nat.*
649 *Geosci.*, 4(3), 195–202, doi:10.1038/ngeo1061, 2011.
- 650 Mackintosh, A. N., Verleyen, E., O'Brien, P. E., White, D. A., Jones, R. S., McKay, R., Dunbar, R., Gore, D. B.,
651 Fink, D., Post, A. L., Miura, H., Leventer, A., Goodwin, I., Hodgson, D. A., Lilly, K., Crosta, X., Golledge, N. R.,
652 Wagner, B., Berg, S., van Ommen, T., Zwartz, D., Roberts, S. J., Vyverman, W. and Masse, G.: Retreat history of
653 the East Antarctic Ice Sheet since the Last Glacial Maximum, *Quat. Sci. Rev.*, 100, 10–30,
654 doi:10.1016/j.quascirev.2013.07.024, 2014.
- 655 Marchant, D. R., Denton, G. H., Swisher, C. C. and Potter, N.: Late Cenozoic Antarctic paleoclimate reconstructed
656 from volcanic ashes in the Dry Valleys region of southern Victoria Land, *Geol. Soc. Am. Bull.*, 108(2), 181–194,
657 doi:https://doi.org/10.1130/0016-7606(1996)108%3C0181:LCAPRF%3E2.3.CO;2, 1996.
- 658 McHargue, L. R. and Damon, P. E.: The global beryllium 10 cycle, *Rev. Geophys.*, 29(2), 141–158,
659 doi:10.1029/91RG00072, 1991.
- 660 Menzies, J., van der Meer, J. J. M. and Rose, J.: Till-as a glacial “tectomict”, its internal architecture, and the

- 661 development of a “typing” method for till differentiation, *Geomorphology*, 75, 172–200,
662 doi:10.1016/j.geomorph.2004.02.017, 2006.
- 663 Michalski, G., Bockheim, J. G., Kendall, C. and Thiemens, M.: Isotopic composition of Antarctic Dry Valley
664 nitrate: Implications for NO_y sources and cycling in Antarctica, *Geophys. Res. Lett.*, 32(13), 1–4,
665 doi:10.1029/2004GL022121, 2005.
- 666 Morgan, D., Putkonen, J., Balco, G. and Stone, J.: Quantifying regolith erosion rates with cosmogenic nuclides 10
667 Be and 26 Al in the McMurdo Dry Valleys, Antarctica, *J. Geophys. Res.*, 115, F03037, doi:10.1029/2009JF001443,
668 2010.
- 669 Nishiizumi, K., Imamura, M., Caffee, M. W., Southon, J. R., Finkel, R. C. and McAninch, J.: Absolute calibration of
670 10Be AMS standards, *Nucl. Instruments Methods Phys. Res. B*, 258, 403–413, doi:10.1016/j.nimb.2007.01.297,
671 2007.
- 672 Paulsen, T. S., Encarnación, J. and Grunow, A. M.: Structure and timing of transpressional deformation in the
673 Shackleton Glacier area, Ross orogen, Antarctica, *J. Geol. Soc. London.*, 161(6), 1027–1038, doi:10.1144/0016-
674 764903-040, 2004.
- 675 Pavich, M. J., Brown, L., Klein, J. and Middleton, R.: 10Be accumulation in a soil chronosequence, *Earth Planet.*
676 *Sci. Lett.*, 68, 198–204, doi:10.1016/0012-821X(84)90151-1, 1984.
- 677 Pavich, M. J., Brown, L., Harden, J., Klein, J. and Middleton, R.: 10Be distribution in soils from Merced River
678 terraces, California, *Geochim. Cosmochim. Acta*, 50, 1727–1735, doi:10.1016/0016-7037(86)90134-1, 1986.
- 679 Pollard, D. and DeConto, R. M.: Modelling West Antarctic ice sheet growth and collapse through the past five
680 million years, *Nature*, 458(7236), 329–332, doi:10.1038/nature07809, 2009.
- 681 Reich, M. and Bao, H.: Nitrate deposits of the Atacama Desert: A marker of long-term hyperaridity, *Elements*,
682 14(4), 251–256, doi:10.2138/gselements.14.4.251, 2018.
- 683 Scarrow, J. W., Balks, M. R. and Almond, P. C.: Three soil chronosequences in recessional glacial deposits near the
684 polar plateau, in the Central Transantarctic Mountains, Antarctica, *Antarct. Sci.*, 26(5), 573–583,
685 doi:10.1017/S0954102014000078, 2014.
- 686 Scherer, R. P., DeConto, R. M., Pollard, D. and Alley, R. B.: Windblown Pliocene diatoms and East Antarctic Ice
687 Sheet retreat, *Nat. Commun.*, 7(1), 1–9, doi:10.1038/ncomms12957, 2016.
- 688 Schiller, M., Dickinson, W., Ditchburn, R. G., Graham, I. J. and Zondervan, A.: Atmospheric 10 Be in an Antarctic
689 soil: Implications for climate change, *J. Geophys. Res.*, 114(F1), 1–8, doi:10.1029/2008jf001052, 2009.
- 690 Spector, P. and Balco, G.: Exposure-age data from across Antarctica reveal mid-Miocene establishment of polar
691 desert climate, *Geol. Soc. Am. | Geol.*, 1, doi:10.1130/G47783.1, 2020.
- 692 Spector, P., Stone, J., Cowdery, S. G., Hall, B., Conway, H. and Bromley, G.: Rapid early-Holocene deglaciation in
693 the Ross Sea, Antarctica, *Geophys. Res. Lett.*, 44(15), 7817–7825, doi:10.1002/2017GL074216, 2017.
- 694 Steig, E., Stuiver, M. and Polissar, P.: Cosmogenic isotope concentrations at Taylor Dome, Antarctica, *Antarct. J.*
695 *United States*, 30, 95–97, 1995.
- 696 Stevens, M. I. and Hogg, I. D.: Long-term isolation and recent range expansion from glacial refugia revealed for the
697 endemic springtail *Gomphiocephalus hodgsoni* from Victoria Land, Antarctica, *Mol. Ecol.*, 12(9), 2357–2369,
698 doi:10.1046/j.1365-294X.2003.01907.x, 2003.
- 699 Stone, J.: A rapid fusion method for separation of beryllium-10 from soils and silicates, *Geochim. Cosmochim.*
700 *Acta*, 62(3), 555–561, doi:10.1016/S0016-7037(97)00340-2, 1998.
- 701 Stroeven, A. P., Prentice, M. L. and Kleman, J.: On marine microfossil transport and pathways in Antarctica during
702 the late Neogene: Evidence from the Sirius Group at Mount Fleming, *Geology*, 24(8), 727–730, doi:10.1130/0091-
703 7613(1996)024<0727:ommtap>2.3.co;2, 1996.

- 704 Sugden, D. E., Marchant, D. R. and Denton, G. H.: The case for a stable East Antarctic ice sheet, *Geogr. Ann. Ser.*
705 *A*, 75(4), 151–351, 1993.
- 706 Talarico, F. M., McKay, R. M., Powell, R. D., Sandroni, S. and Naish, T.: Late Cenozoic oscillations of Antarctic
707 ice sheets revealed by provenance of basement clasts and grain detrital modes in ANDRILL core AND-1B, *Glob.*
708 *Planet. Change*, 96–97, 23–40, doi:10.1016/j.gloplacha.2009.12.002, 2012.
- 709 Valletta, R. D., Willenbring, J. K., Lewis, A. R., Ashworth, A. C. and Caffee, M.: Extreme decay of meteoric
710 beryllium-10 as a proxy for persistent aridity, *Sci. Rep.*, 5, 17813, doi:10.1038/srep17813, 2015.
- 711 Webb, P. N. and Harwood, D. M.: Late Cenozoic glacial history of the Ross embayment, Antarctica, *Quat. Sci.*
712 *Rev.*, 10(2–3), 215–223, doi:10.1016/0277-3791(91)90020-U, 1991.
- 713 Webb, P. N., Harwood, D. M., McKelvey, B. C., Mercer, J. H. and Stott, L. D.: Cenozoic marine sedimentation and
714 ice-volume variation on the East Antarctic craton, *Geology*, 12(5), 287–291, doi:10.1130/0091-
715 7613(1984)12<287:cmsaiv>2.0.co;2, 1984.
- 716 Webb, P. N., Harwood, D. M., Mabin, M. G. C. and McKelvey, B. C.: A marine and terrestrial Sirius Group
717 succession, middle Beardmore Glacier-Queen Alexandra Range, Transantarctic Mountains, Antarctica, *Mar.*
718 *Micropaleontol.*, 27(1–4), 273–297, doi:10.1016/0377-8398(95)00066-6, 1996.
- 719 Welch, K. A., Lyons, W. B., Whisner, C., Gardner, C. B., Gooseff, M. N., Mcknight, D. M. and Priscu, J. C.: Spatial
720 variations in the geochemistry of glacial meltwater streams in the Taylor Valley, Antarctica, *Antarct. Sci.*, 22(6),
721 662–672, doi:10.1017/S0954102010000702, 2010.
- 722 Willenbring, J. K. and von Blanckenburg, F.: Meteoric cosmogenic Beryllium-10 adsorbed to river sediment and
723 soil: Applications for Earth-surface dynamics, *Earth-Science Rev.*, 98(1–2), 105–122,
724 doi:10.1016/j.earscirev.2009.10.008, 2010.
- 725 Wilson, G. S.: The neogene east antarctic ice sheet: A dynamic or stable feature?, *Quat. Sci. Rev.*, 14(2), 101–123,
726 doi:10.1016/0277-3791(95)00002-7, 1995.
- 727 You, C. F., Lee, T. and Li, Y. H.: The partition of Be between soil and water, *Chem. Geol.*, 77(2), 105–118,
728 doi:10.1016/0009-2541(89)90136-8, 1989.
- 729